博士論文

論文題目

C-terminal-truncating *ASXL1* mutations induce MDS via inhibition of PRC2

(*ASXL1* 遺伝子の C 末端欠失型変異は PRC2 を阻害し MDS を惹起する)

氏名　井上　大地

Abstract

Owing to genome-wide sequencing efforts in the last decade, recurrent mutations in epigenetic regulators are found in various myeloid malignancies. In particular, *ASXL1* mutations are frequently found in patients with hematological malignancies associated with myelodysplasia including myelodysplastic syndromes (MDS), and chronic myelomonocytic leukemia and are found to be associated with poor prognosis. Although loss-of-function *ASXL1* mutations promote myeloid transformation, a large subset of *ASXL1* mutations is thought to result in stable truncation of ASXL1. Here we demonstrate that C-terminal truncating *ASXL1* mutations (ASXL1-MT) inhibit myeloid differentiation and induce MDS-like disease in mice, displaying all the features of human MDS including multi-lineage myelodysplasia, pancytopenia and occasional progression to overt leukemia. Concerning the molecular mechanisms, ASXL1-MT derepressed expression of *Hoxa9* and miR-125a through inhibiting PRC2-mediated methylation of H3K27 in a dominant negative fashion. miR-125a targeted expression of a surface receptor *Clec5a*, which was found to contribute to myeloid differentiation. In addition, *HOXA9* expression was high in MDS patients with ASXL1 mutations while

CLEC5A expression was generally low in MDS patients. Thus, ASXL1-MT induced MDS-like disease in mice associating with derepression of *Hoxa9* and miR-125a, and *Clec5a* downregulation. Our data provide evidence for a novel axis of MDS pathogenesis (*ASXL1* mutations-upregulation of *HOXA9* and miR-125a-downregulation of *CLEC5A*) and implicate the involvement of PRC2 in myeloid transformation.

Introduction

An appropriate regulation of gene expression is vital to allow every and each one of cells to function in the right manner. Epigenetics is the study of clarifying changes in gene expression or cellular phenotype during development, differentiation, or oncogenesis, caused by mechanisms independently of direct changes of DNA nucleotide sequences. Epigenetic changes refer to functionally relevant modifications to the nucleotide or histone proteins adjacent to the genome. Examples of such modifications are DNA methylation and histone modification, both of which lead to regulate gene expression (1). DNA methylation is an important regulator of gene transcription and a large subset of evidence has demonstrated that genes with high levels of 5-methylcytosine in their promoter region are transcriptionally silent, and that DNA methylation gradually accumulates upon long-term gene silencing (2, 3). In fact, DNA methylation is essential during normal development, and patterns of DNA methylation in somatic cells are generally inherited to daughter cells with a high fidelity (4). Of note, aberrant DNA methylation patterns, including hypermethylation at the promoter region and global hypomethylation compared to normal tissues, have been associated with a

large number of human malignancies (5-10). Hypermethylation typically occurs at CpG islands in the promoter region and is related to gene inactivation. On the other hand, the pattern of histone modifications also plays an important role in gene expression. Histones H2A, H2B, H3 and H4 are known as the core histones in eukaryotic cell nuclei (11). Two H2A-H2B dimers and a H3-H4 tetramer assemble to form one octameric nucleosome core particle, and 146 base pairs of DNA wrap around this core particle 1.75 times (11-13). The amino acid residues of histones are subject to post translational modification by site-specific enzymes such as lysine methylation, arginine methylation, lysine acetylation, serine/threonine/tyrosine phosphorylation, and lysine ubiquitination (4, 14-16). Histone modifications have been found to alter the electrostatic charge of the histone resulting in a structural change in histones or their binding to DNA, leading to the change of accessibility to regulatory proteins (17). Combinations of histone modifications are thought to constitute a code, the so-called “histone code” (18, 19). The histone code hypothesis suggests that information is 'written' by site-specific enzymes that introduce or remove covalent modifications from the flexible N-terminal tails of histones (20). This information is then interpreted by 'readers'—that is, effector domains of proteins that recruit machinery required to stabilize or remodel specific

chromatin states (20). Overall, posttranslational modifications of histones create an epigenetic mechanism for the regulation of a variety of normal and disease-related processes. Most well-studied histone modifications related to transcription are following. Trimethylation of H3 lysine 4 (H3K4me3) mediated by trithorax group (TrxG) is representative active mark, while monoubiquitination of H2A lysine 119 (H2AK119Ub) by polycomb-group repressive complex 1 (PRC1) and trimethylation of H3 lysine 27 (H3K27me3) by PRC2 are repressive marks (Figure 1) (1). Thus, the actions of TrxG proteins are often described as antagonistic of PRC proteins function.

Additional sex combs (*Asx*) is an Enhancer of Trithorax and Polycomb (ETP) group gene in *Drosophila* (21, 22). *Asx* deletion results in a homeotic phenotype characteristic of both Polycomb group (PcG) and TrxG gene deletions, which led to the hypothesis that Asx has dual functions in silencing and activation of homeotic gene expression (22, 23). *Additional sex combs-like1* (*ASXL1)* is one of three mammalian homologs of the Drosophila *Additional sex combs* (*Asx*), and plays critical roles both in activation and suppression of *Hox* genes in axial patterning through regulating the PcG and TrxG proteins (24-27). Actually, Fisher et al demonstarated that the embryos of a loss-of-function Asxl1 mutant mouse model exhibited simultaneous anterior and

posterior transformations of the axial skeleton, consistent with a role for Asxl1 in activation and silencing of *Hox* genes (24). Of interest, it has been recently reported that heterozygous de novo nonsense mutations in *ASXL1*, similarly to those found in MDS patients, can be identified in a rare congenital disease of human, Bohring-Opitz syndrome, characterized by severe intellectual disability, distinctive facial features and multiple congenital malformations (28), although MDS-like disease has not been reported in this syndrome due to the lethality in early childhood.

All mammalian ASXL proteins have conserved sequence features: an amino-terminal ASX homology (ASXH) region, which contains 2 putative nuclear receptor coregulator binding (NR box) motifs, 3 other NR box motifs, and a carboxyterminal plant homeodomain (PHD) domain (Figure 2) (29). The region around the ASXH domain is required for binding the PcG protein Calypso, which has histone deubiquination activity in contrast to PRC1 (30). This function is conserved in mammals because the ASXH domain of ASXL1 interacts with BRCA1 associated protein-1 (BAP1), the mammalian homolog of Calypso (30). The region around ASXH domain also promotes binding between ASXL1 and lysine (K)-specific demethylase 1A (KDM1A) or heterochromatin protein 1A (HP1a), which are required for repressing retinoic acid-receptor (RAR) and

the retinoid X receptor (RXR) activities (31). NR binding motifs act together with chromatin-remodeling factors, coactivators and corepressors to regulate gene transcription (32). The PHD domain, located in the C-terminus of ASXL1, is a histone or DNA binding module for transcription factor and chromatin regulators (33). In addition, recent bioinformatics analysis of the conserved domains of mammalian ASXL proteins has suggested that the N-terminal domain of ASXL1 (amino acids 10–100) might represent a unique DNA binding motif, termed a HARE-HTH domain (HB1, ASXL1, restriction endonuclease helix-turn helix domain) (34). As described above, ASXL1 functions as a co-repressor of RAR activity in mammalian cell lines that are retinoic acid (RA) resistant, while ASXL1 also has been shown to function as a transcriptional co-activator of RAR and RXR in human RA-sensitive cancer cell lines (26). These results support dual activator/repressor functions for mammalian ASXL1 proteins depending on cellular context and that mammalian ASXL1 proteins have dual functions, similarly to *Drosophila* Asx proteins.

Recently it was reported that ASXL1 binds members of PRC2, specifically enhancer of zeste homolog 2 (EZH2), embryonic ectoderm development (EED) and suppressor of zeste 12 homolog (SUZ12), and that ASXL1 loss in myeloid hematopoietic cells

profoundly inhibits tri-methylation of H3K27, a hallmark repressive modification induced by the PRC2 (Figure 3) (35). In addition, as described above, ASXL1 also associates with BAP1, a nuclear-localized deubiquitinase, which may promote expression of genes (36) through removal of H2A lysine 119 ubiquitination placed by the PRC1 complex. Thus, ASXL1 appears to be involved in both PRC2-mediated gene repression and opposition of PRC1 function (37).

From another point of view, genome-wide sequencing efforts in the last decade, targeted for the patients' samples with myeloid malignancies, have identified a series of mutations in unknown epigenetic regulators, including *ASXL1*, *EZH2* and *Tet Methylcytosine Dioxygenase 2* (*TET2*) (38, 39). Surprisingly, *ASXL1* is mutated in patients with the entire spectrum of myeloid malignancies including 11—21% of patients with myelodysplastic syndromes (MDS) (40-43), 10—15% of patients with myeloproliferative neoplasms (MPN), 5—25% of patients with acute myeloid leukemia (AML) (40, 42), and 43—58% of patients with chronic myelomonocytic leukemia (CMML) (41, 42, 44, 45). Of important, in several clinical studies, mutations in *ASXL1* appear to be novel biomarkers of adverse overall survival in patients with MDS and acute myeloid leukemia, independent from other clinically utilized prognosticators (43,

44). However, how the mutant forms of ASXL1 contribute to the development of myeloid malignancies remains to be elucidated.

MDS is a heterogeneous group of clonal stem-cell disorders characterized by dysplastic bone marrow (BM) morphology, variable cytopenias, ineffective hematopoiesis, increased risk of transformation to AML and poor progonisis (46, 47). Although stem cell transplantation, particularly for younger patients, is the one way to overcome the disease, MDS affects mainly in elderly (48). Recently, DNA hypomethylating agents like azacitidine, immunomodulating agents such as lenalidmide, and histone deacetylase inhibitors (HDACi) have been shown to be promising agents against MDS even though these agents have difficulty in curing MDS patients, suggesting that epigenetic abnormality caused by genetic mutations is a key to understanding molecular mechanism for myeloid transformation and disease development (49, 50). Thus, clarifying the underlying mechanism for MDS pathogenesis caused by *ASXL1* mutations is a critical issue to be solved.

Although loss of ASXL1 promotes myeloid transformation by impairing PRC2-mediated gene repression at a number of critical loci (35), intriguingly, most *ASXL1* mutations are located in the 5’ region of the last exon (exon 12), which are

predicted to result in expression of a truncated ASXL1 protein. As further support for this, *ASXL1* mutations are usually heterozygous, leaving one allele intact. Therefore, we hypothesized that the C-terminal truncated form of ASXL1 might function as a dominant-negative mutant that suppresses the wild-type ASXL1 function or alternatively as a gain-of-function mutant (51, 52). These possible effects of *ASXL1* mutations have not been studied and are critical to delineate given the clinical importance of *ASXL1* mutations.

In this study, we have shown that *ASXL1* mutations profoundly inhibited myeloid differentiation *in vitro* and induced typical MDS in a mouse model. We then sought to explore the molecular link between *ASXL1* mutations and epigenetic disturbances which lead to development of MDS. We identify that expression of mutant forms of ASXL1 results in impaired PRC2-function and impairment of myeloid differentiation *in vitro* and *in vivo*. Moreover, we identify that *ASXL1* mutations induce upregulated expression of miR-125a and subsequent suppression of *C-type lectin domain family 5, member a* (*Clec5a*), a type II membrane protein critical for myeloid differentiation. These results identify a novel genetically-accurate murine model of MDS and additional critical pathways for *ASXL1*-mediated myeloid transformation. Moreover, these findings

suggest novel therapeutic potential for targeting the mutant forms of ASXL1 as well as miR-125 in the treatment of patients with myeloid malignancies.

Methods

Mice

C57BL/6 (Ly5.1) mice (Sankyo Labo Service Corporation) and C57BL/6 (Ly5.2) mice (Charles River Laboratories Japan) were used for bone marrow transplantation experiments.

Cell Culture

HEK293T cells were cultured in Dulbecco's modified Eagle's medium (DMEM) supplemented with 10% fetal bovine serum (FBS). Human leukemia cell lines were cultured in RPMI-1640 supplemented with 10% FBS (HL60, U937, K562, KU812, TS9;22, and MEG-01 cells), RPMI-1640 supplemented with 20% FBS (SET2, NOMO1 and Mono-Mac-6 cells), RPMI-1640 medium supplemented with 10% FBS+1 μM hydrocortisone+10% horse serum (UKE1 cells) or IMDM with 20% FBS (KBM5 cells). The murine myeloid cell lines 32Dcl3 and FDC-P1 were grown in RPMI 1640 medium supplemented with 10% FBS, antibiotics, L-glutamine, and 1 ng/ml of interleukin-3 (IL-3). Before the assays for proliferation and differentiation, the transduced 32Dcl3,

HL60, or FDC-P1 cells were GFP-sorted or subjected to drug selection with 1 μg/mL puromycin and/or 10 μg/mL blasticidin, if necessary.

Vector construction

We used the retrovirus vectors pMYs-FLAG-tagged-ASXL1-WT-IG and pMYs-FLAG-tagged-ASXL1-MT-IG in which a wild-type or a mutant ASXL1 (1934dupG; G646WfsX12 and 1900-1922del; E635RfsX15), tagged with a FLAG epitope at the N terminus, was inserted upstream of the internal ribosome entry site-enhanced green fluorescent protein (IRES-EGFP) cassette of pMYs-IG (53). Similarly, wild-type Clec5a or Clec5a-K16A was inserted upstream of the IRES-puro to generate pMYs-Clec5a-IP or pMYs-Clec5a-K16A-IP. ASXL1-MT was subcloned upstream of the IRES-blasticidin cassette of pMYs-IB. Likewise, Myc-tagged EZH2 was subcloned into pMYs-IG to generate pMYs-Myc-tagged-EZH2-IG. To perform the mouse BMT model, we constructed pMYs-N-Ras-G12V-IG and pMYs-ASXL1-MT-IRES-NGFR (nerve growth factor receptor). For knock-down assays, shRNA expression fragments were cloned into pMXs-U6-GFP or pMXs-U6-Puro, which were pMXs-based self-inactivating retrovirus vectors expressing

shRNA under a U6 promoter with a PGK promoter-driven GFP or puromycin-resistant gene expression. The sequences of shRNA are described in Table 1. An shRNA expression cassette was constructed in the opposite direction from a GFP/Puro expression cassette. We also constructed microRNA vectors as described previously (54). Briefly, microRNA expression fragments were cloned into pMXs-EF1-Puro vector.

Transfection and retrovirus production

Retroviral production was done as described previously (55). Briefly, retroviruses were generated by transient transfection of Plat-E packaging cells with using the calcium-phosphate coprecipitation method. Cell lines such as 32Dcl3 were infected with the retroviruses as previously described (53).

Mutation analysis of *ASXL1*

Somatic mutations of *ASXL1* genes were searched by sequencing exons after polymerase chain reaction (PCR) amplification of genomic DNA as described previously (41).

Real-time PCR (qRT-PCR)

Total RNAs were treated with Deoxyribonuclease I (Invitrogen, Carlsbad, CA, USA) and reverse transcribed by using High Capacity cDNA Reverse Transcription Kits (Applied Biosystems, Carlsbad, CA, USA) or miScript Reverse Transcription Kit (QIAGEN, Hilden, Germany). qRT-PCR was performed using a Rotor-Gene Q (QIAGEN). For mRNA real-time PCR, a SYBR Premix EX Taq (Takara, Shiga, Japan) was used as described (56). The primer sets for qRT-PCR are described in Table 2. Mature miR-125a expression was measured using a miScript SYBR Green PCR kit (QIAGEN). cDNA was amplified with miR-125a-specific primers (QIAGEN). Expression of RNU6B (RNA, U6 small nuclear 2), as an internal control, was used for normalization of the results. All data with error bars are presented as mean ± SEM.

Mouse BMT

Mouse BMT was performed as described previously (55). Briefly, BM mononuclear cells were isolated from the femurs and tibias of C57BL/6 (Ly-5.1) donor mice three days after intraperitoneal administration of 150 mg/kg 5-fluorouracil. The cells were

stimulated with 50 ng/mL of mouse stem cell factor, mouse FLT3 ligand, mouse IL-6, and human thrombopoietin (all cytokines were from R&D Systems). The prestimulated cells were infected for 60 hours with the retroviruses harboring pMYs-IG, pMYs-FLAG-ASXL1-MT-IG, pMYs-FLAG-ASXL1-WT-IG, pMYs-N-Ras-G12V-IG and pMYs-INGFR, or pMYs-N-Ras-G12V-IG and pMYs-ASXL1-MT-IRES-NGFR, using 6-well dishes coated with RetroNectin (Takara Bio). Then, 2×10^6 of the infected BM cells were injected into sublethally γ-irradiated C57BL/6 (Ly-5.2) recipient mice. Overall survival of transplanted mice was estimated using the Kaplan-Meier method. All animal studies were approved by the Animal Care Committee of the Institute of Medical Science, The University of Tokyo.

Flow cytometric analysis

Cells were stained with indicated phycoerythrin-conjugated antibodies (eBioscience). Flow cytometric analysis of the stained cells was performed with FACS Caliburflow (BD Biosciences) equipped with FlowJo Version 7.2.4 software (TreeStar). All data with error bars are presented as mean ± SEM.

Analysis of cell growth

Cell growth was estimated by CellTiter-Glo™ Luminescent Cell Viability Assay (Promega, Madison, WI, USA). All data with error bars are presented as mean ± SEM.

Immunostaining

Immunostaining of HEK293T cells transiently transfected with retrovirus constructs was performed as described previously (57). After fixation with 1.5% paraformaldehyde, cells were immunostained with rabbit anti-Flag Ab. The cells were then stained with Alexa Fluor 546–conjugated goat anti–rabbit immunoglobulin G secondary Ab (Molecular Probes). Nuclei were counterstained with DAPI (4', 6-Diamidino-2-phenylindole dihydrochloride). Fluorescent images were analyzed on a confocal microscope (FLUOVIEW FV300 scanning laser biological microscope JX70 system; Olympus) equipped with SenSys/0L cold charge-coupled device (CCD) camera (Olympus). An LCPlanFI ×60/1.40 NA oil was used as the objective lens. Data are representative of three independent experiments.

Western blot analysis

Cell lysates were subject to immunoblotting using the following antibodies: ASXL1 (Clone 2049C2a; Santa Cruz (sc-81053); C-terminus directed), EZH2 (Clone AC22; Cell Signaling Technologies #3147), FLAG (M2 FLAG; Sigma A2220), c-myc (Clone 9E10; Roche 11 667 203 001), H3K27me3 (CMA323) (58), total histone H3 (59), and tubulin (Clone B-5-1-2; Santa Cruz sc-23948). Antibodies different from the above used for immunoprecipitation include anti-EZH2 antibodies (Active Motif 39901). Immunoprecipitation was performed in an immunoprecipitation buffer (150 mM NaCl, 50 mM Tris (pH 7.5), 1 mM EDTA, 1% Triton, 2 mM sodium orthovanadate, 2 mM PMSF, 50mM sodium fluoride). Western blot analysis of purified histone was performed as described previously (60). Data are representative of three independent experiments.

Chromatin immunoprecipitation (ChIP) assay

ChIP assays were performed as described previously (58) except for the process of cross-link and quenching reactive aldehydes. In brief, 32cl3 cells or sorted bone marrow cells ($2\text{-}5\times10^6$) were cross-linked with 1% formaldehyde for 5 min at room temperature and then incubated with 350mM glycine for 5 min for quenching. These assays were

carried out using the following antibodies: EZH2 (Active motif 39901), H3K4me3 (CMA304), H3K9me3 (CMA318), H3K27me3 (CMA323) (58), and ubiquityl-histone H2AK119 (Clone D27C4; Cell Signaling Technologies 8240). Quantitative PCR was performed with a Rotor-Gene Q (QIAGEN) using SYBR Premix EX Taq (Takara, Shiga, Japan). The primer sets for quantitative PCR are described in Table 3. All data with error bars are presented as mean ± SEM. Data are representative of three independent experiments.

Differentiation Assay

The 32Dcl3 cells were induced to differentiate to granulocytes by removing IL-3, washing them twice in RPMI medium without IL-3, and adding granulocyte colony-stimulating factor (G-CSF) (R & D Systems) to a final concentration of 50 ng/ml. Cells were cytocentrifuged (Cytospin4, Thermo Shandon, Pittsburgh), and cell morphologies were evaluated by Giemsa staining three or six days after G-CSF addition (61). FDC-P1 cells were washed in RPMI medium and then incubated in mGM-CSF (10 ng/mL) for six days (62). HL60 cells were incubated in the medium supplemented with 10^{-6}M ATRA for three days. Images were obtained with a BX51 microscope and a

DP12 camera (Olympus); objective lens, UplanFl (Olympus). All data with error bars are presented as mean ± SEM. Data are representative of three independent experiments.

Microarray analysis

BM cells derived from mock-transplanted mice and ASXL1-MT transplanted mice were incubated with biotinylated antibodies for CD3e, B220, and TER-119, followed by incubation with streptavidin Micro Beads (Miltenyi Biotec). The described marker-negative fraction was separated with LS Columns (Miltenyi Biotec). Using 32Dcl3 cells transduced with pMYs-IG and pMYs-FLAG-ASXL1-MT-IG and sorted-BM cells, total RNA was extracted by Trizol reagent (Invitrogen) according to the manufacturer's protocol. Double-stranded cDNA was synthesized from 5 μg of total RNA with oligo (dT)24 T7 primer, amplified with T7 RNA polymerase up to approximately 50 μg of cRNA, and hybridized to Affymetrix Mouse Expression array 430A, which contains 45000 probe sets for 39000 transcripts and variants from over 34000 well-characterized mouse genes (Affymetrix). After washing and staining, the arrays were scanned on the GeneChip system confocal scanner (Affymetrix). The

intensity for each feature of the array was captured with Affymetrix Microarray Suite (MAS) Version 5.0 software. Gene set enrichment analysis was performed by using Gene Ontology gene sets from the Molecular Signatures Database (http://www.broad.mit.edu/gsea/msigdb/) (63).

Luciferase assay

Luciferase assays to investigate whether microRNA binds to the expected target sequence were performed as described previously (54). All data with error bars are presented as mean ± SEM.

Statistical analysis

Statistical significance was calculated using the indicated tests for independent variables. All calculations were carried out using the program JMP 8.0 (SAS Institute Inc., Cary, NC, USA). *P*-values (*) of < 0.05 were considered significant using two tailed Student's t-test, unless otherwise noted. In box and whisker plots, the bottom and top of the box indicates the first and third quartiles, and the band inside the box is the second quartile (the median). The lowest or highest datum shows the minimum or maximum of all of

the data within 1.5 interquartile range (IQR) of the lower or upper quartile.

Study approval

All animal studies were approved by the Animal Care Committee of the Institute of Medical Science, The University of Tokyo. MDS patients were diagnosed at Hannover Medical School. Diagnosis was based on the World Health Organization classification. Informed consent was obtained in accordance with the Declaration of Helsinki, and the studies were approved by the institutional review board of Hannover Medical School (Ethical vote No. 5558) and by the ethics committees of the University of Tokyo (Approval no. 20-10).

Results

Mutant ASXL1 inhibited G-CSF-induced differentiation of 32Dcl3 cells

Most *ASXL1* frame-shift mutations are found in the last exon, which are predicted to result in expression of C-terminal truncated forms, because nonsense-mediated mRNA decay (NMD) cannot occur in case of the mutation of the last exon (64). We constructed an N-terminal FLAG-tagged truncated mutants of ASXL1, FLAG-ASXL1-MT1 and MT2 as well as N-terminal FLAG-tagged wild type ASXL1 (FLAG-ASXL1-WT) (Figure 2). FLAG-ASXL1-MT1 and MT2 were derived from the mutated gene of 1934dupG;G646WfsX12 and 1900-1922del;E635RfsX15 of patients with MDS, respectively. Although there is some controversy as to whether the most common *ASXL1* mutation 1934dupG;G646WfsX12 represents a true somatic mutation or an artifact (65), most studies have suggested this allele can occur as a somatic mutation in hematologic malignancies (66-68). When transiently expressed in HEK293T cells or stably expressed in 32Dcl3 cells, these constructs expressed ASXL1 wild-type (ASXL1-WT) and mutant proteins (ASXL1-MTs) with expected molecular weights detected by an anti-FLAG antibody (Figure 4). As reported (35), immunoprecipitation

studies demonstrated that EZH2 bound ASXL1-WT. We further demonstrated that ASXL1-MT as well as ASXL1-WT can bind to EZH2 (Figure 5). ASXL1-WT could also be detected in hemopoietic cell lines by anti-C-terminal ASXL1 antibodies (Figure 6); HL60, U937, and SET2 harboring only the wild-type ASXL1 alleles expressed the wild-type 190 kDa protein. In K562, KU812, and Mono-Mac-6 harboring one wild-type and one truncated mutant, ASXL1-WT could be easily detected with the C-terminal antibody. To detect C-terminal truncated endogenous ASXL1 proteins, we used antibodies against the N-terminal part of ASXL1. However, the backgrounds were so high that we could not determine whether the C-terminal truncated ASXL1 was expressed. Similarly, in TS9;22, KBM-5, and MEG-01 cell lines harboring homozygous truncated ASXL1, we were not able to determine whether the truncated ASXL1 was expressed. Thus, we confirmed by qRT-PCR that *ASXL1* transcripts were detected in these cell lines with or without *ASXL1* mutations (Figure 7). When ASXL1-MTs, which harbors 3 putative nuclear localization signals (NLSs), were expressed in HEK293T cells, they localized to the nucleus (Figure 2 and 8) as the ASXL1-WT. These data suggested that the truncated ASXL1 mutant is expressed and prompting us to consider that the C-terminal truncated form of ASXL1 works as a dominant negative mutant

suppressing the wild-type ASXL1 or gain-of-function mutant (51, 52).

Next, we investigated the effects of expression of wild-type and mutant ASXL1 alleles on hematopoietic differentiation. To this end, we expressed ASXL1-MT1 and MT2 in 32Dcl3 and examined their effect on differentiation of the transduced cells. Interestingly, G-CSF-induced differentiation of 32Dcl3 cells was inhibited by the expression of ASXL1-MT1 and MT2 but not by the expression of ASXL1-WT, based on morphology and flow-cytometric expression of CD11b (Figure 9). In addition, all-trans-retinoic acid (ATRA)-induced granulocytic differentiation of HL60 and GM-CSF-induced monocytic differentiation of FDC-P1 cells were attenuated by the overexpression of ASXL-1-MT2 (Figure 10). The expression of ASXL1-MTs as well as ASXL1-WT did not affect the growth rate of 32D cells cultured in the presence of IL-3 and did not induce factor independent growth (Figure 11). For further experiments, we mainly used ASXL1-MT2 unless otherwise specified, calling this mutant ASXL1-MT.

ASXL1-MT reduced the expression of *Clec5a/Mdl1*

To elucidate the molecular mechanisms by which the ASXL1-MT inhibited the G-CSF-induced differentiation of 32Dcl3, we compared the expression profiles of

parental 32Dcl3 cells and 32Dcl3 cells expressing ASXL1-MT maintained in the presence of 1 ng/ml IL-3 or 50 ng/ml G-CSF. We identified a small set of genes whose expression levels changed more than two fold. These included *Clec5a/Mdl1*, *Cd14*, and *Prom1*. Expression of these genes was downregulated in 32Dcl3 cells expressing the ASXL1-MT. Among them, we focused on the type II transmembrane receptor Clec5a (69), because it was known that Clec5a expression is associated with granulocytic differentiation of 32Dcl3 cells (70). We confirmed that expression of *Clec5a* was reduced in 32Dcl3 expressing ASXL1-MT (Figure 12). Moreover, while the expression of Clec5a in 32D cells was increased by G-CSF stimulation in a time-dependent manner as reported (70) both in mRNA and protein levels, this increase was profoundly suppressed by the expression of ASXL1-MT but not by ASXL1-WT (Figure 12 and 13). This may result from the observations that myeloid differentiation of 32Dcl3 cells was inhibited by ASXL1-MT, and expression of Clec5a increases with myeloid differentiation suggesting Clec5a serves as a marker of myeloid differentiation. On the other hand, ATRA or G-CSF-induced granulocytic differentiation of HL60 cells or 32Dcl3cells, respectively, was enhanced by the expression of Clec5a (Figure 14 and Figure 15), suggesting that Clec5a plays a direct role in the differentiation of myeloid

cells.

To examine the direct involvement of Clec5a in G-CSF-induced differentiation of 32Dcl3 cells, we designed two small hairpin RNAs (shRNAs; sh3 and sh4) for *Clec5a*, which efficiently knocked down Clec5a expression in 32Dcl3 cells (Figure 16 and 17). Intriguingly, G-CSF-induced differentiation of 32Dcl3 was significantly inhibited by Clec5a knock-down (Figure 18), suggesting that ASXL1-MT inhibits differentiation of 32Dcl3 cells, at least in part, through suppression of Clec5a. Importantly, ectopic expression of Clec5a in ASXL1-MT expressing 32Dcl3 cells restored the differentiation ability of 32Dcl3, although this restoration was not induced by a mutant Clec5a that harbors a K16A mutation in the transmembrane domain which disrupts the ability to associate with DAP12 (Figure 19), an activating adaptor for Clec5a that transmits the positive signal associating with Clec5a (Figure 20, 21, and 22) (69). Thus, ASXL1-MT reduced the expression of Clec5a, which contributes to granulocytic differentiation of 32Dcl3 cells, leading to the disturbed differentiation of 32Dcl3 cells. Interestingly, expression of *CLEC5A* was reduced in the whole BM cells of the majority of patients with MDS when compared with normal BM cells (Figure 23). However, the presence or absence of *ASXL1* mutations did not correlate with *CLEC5A* expression in BM cells of

MDS patients, suggesting that other MDS disease alleles can alter *CLEC5A* expression in *ASXL1* wild-type patients.

ASXL1-MTs induced MDS-like disease in mice

Using a mouse bone marrow transplant (BMT) model, we next examined the *in vivo* effect of ASXL1-MT expression. BM cells derived from 5-fluorouracil-treated Ly5.2 mice were transduced with a retrovirus vector pMXs-FLAG-ASXL1-MT2-IG (IRES-GFP), and the transduced cells were transplanted into sublethally irradiated Ly5.1 mice. In the transplanted mice, the percentage of the GFP-positive cells gradually increased in the peripheral blood and reached 41-100% one year after transplantation, while it gradually decreased over time in the mice transplanted with ASXL1-WT- or empty vector-transduced BM cells (Figure 24). GFP-positive cells in the BM of ASXL1-MT-transduced mice 6 months after the transplantation were mostly CD11b-positive and included relatively few B220-positive cells while GFP-negative non-transduced cells consisted of equal numbers of CD11b-positive and B220-positive cells (Figure 25). All of the transplanted mice displayed more or less morphological abnormalities 12 months or later after transplantation, mainly in myeloid cells and red

blood cells (Figure 26), including Pelger-Huet anomaly and hypersegmentation for myeloid cells and Howel-Jolly bodies, polychromasia and anisopoikilocytosis for erythrocytes, consistent with multi-lineage dysplasia of human MDS. Mice expressing ASXL1-MT died of severe anemia after a long latency (median survival, 400.5 days) while some of ASXL1-MT transduced mice suffered from leukemic transformation (Figure 27). On the other hand, most of the mock-transduced mice survived nearly two years without developing myeloid malignancies (Figure 27). GFP-positive BM cells increased in ASXL1-MT-transduced mice were positive for CD11b, and weakly positive for Gr1 and CD34. Expression of c-kit varies from positive to negative. These data suggest that GFP-positive population contain immature and mature myeloid cells (Figure 28). These mice developed severe anemia, leukopenia, and thrombocytopenia while the BM was hypercellular and the spleen was enlarged (Figure 29 and 30). Thus, ASXL1-MT-transduced MDS mice developed pancytopenia with dysplasia in granulocytes and erythroid cells and occasionally progressed to overt leukemia, displaying all the features of human MDS. Overexpression of ASXL1-MT1 in the same BMT model, revealed basically identical results (Figure 31).

Expression profiles of hemopoietic cells of the mice that developed MDS

To elucidate the molecular mechanisms by which ASXL1-MT induced MDS, we performed expression profiles of BM cells of mice that developed MDS. We used CD3-/B220-/Ter119- BM cells of mock-transduced mice as a control. Gene set enrichment analysis (GSEA) indicated that ASXL1-MT induced an expression profile which inversely correlated with known PRC target genes (71), suggesting that ASXL1-MT inhibited PRC (Figure 32). We also examined the expression of *Hoxa* genes and *Clec5a* in BM cells of the mice that developed MDS or MDS/AML after transplantation of ASXL1-MT-transduced BM cells; the expression of posterior *Hoxa* genes was increased and that of *Clec5a* was decreased in BM cells of MDS or MDS/AML mice when compared to BM cells of mock-transduced mice (Figure 33). We next performed chromatin immunoprecipitation (ChIP) of the promoter regions of posterior *Hoxa* genes using H3K27me3 antibodies, and found that H3K27me3 was greatly decreased around the promoter regions of *Hoxa5*, *Hoxa9*, and *Hoxa10* in the MDS mice, correlating well with the upregulation of their mRNA expression (Figure 33 and 34). In addition, Western blot analysis of purified histones in 32Dcl3 cells transduced with ASXL1-MT indicated that H3K27me3 was reduced globally (Figure

35). To clarify the mechanisms by which ASXL1-MT reduced H3K27me3, we tested the binding between ASXL1 and EZH2. As described above, immunoprecipitation studies demonstrated that EZH2 bound ASXL1-WT. EZH2 also bound ASXL1-MT (Figure 5). Importantly, co-expression of ASXL1-MT with ASXL1-WT efficiently inhibited the binding between ASXL1-WT and EZH2; at expression levels similar to ASXL1-WT, ASXL1-MT nearly eliminated the binding of ASXL1-WT to EZH2 (Figure 36). This result suggested a dominant-negative role of ASXL1-MT in PRC2 function. Although we also tried to investigate whether ASXL1-MT blocked the binding of ASXL1-WT to genome or genome-binding PRC2 using ChIP assay, we found it difficult to detect ASXL1 proteins on genome because ASXL1 proteins were easily degraded by proteasome in the procedure.

Interestingly, *HOXA9* expression was increased in whole BM cells of most MDS patients harboring *ASXL1* mutations while the changes in *HOXA9* expression was not significant in MDS patients without *ASXL1* mutations (Figure 37).

ASXL1-MT collaborated with N-Ras-G12V in inducing leukemia

ASXL1 mutations are known to frequently co-occur with N/K-RAS mutations in

myeloid malignancies and ASXL1 knockdown reduces the latency and increases the severity of myeloproliferation induced by N-Ras-G12D (35). We thus examined whether stable expression of ASXL1-MT might similarly collaborate with N-Ras-G12V *in vivo*. As reported, N-Ras-G12V induced MPN-like diseases in the BMT model (72). In this model, co-transduction of ASXL1-MT, but not ASXL1-WT, with N-Ras-G12V significantly shortened latency when compared with mice transplanted with BM cells transduced with N-Ras-G12V alone (Figure 38) and increased the number of immature blast (35% vs. 15%), indicating that the combination of N-Ras-G12V and ASXL1-MT induced progression to AML rather than MPN (Figure 39 and 40). It also enhanced hepatosplenomegaly in the affected mice (Figure 41 and 42), while hemoglobin concentrations and number of white blood cells did not change significantly (Figure 43). The expression of *Hoxa9* was increased in leukemic cells induced by ASXL1-MT and N-Ras-G12V when compared to that in MPN cells induced by N-Ras-G12V alone (Figure 44), suggesting that ASXL1-MT inhibited PRC2-driven repression of transcription. On the other hand, expression of *Clec5a* was significantly decreased in leukemic cells induced by ASXL1-MT and N-Ras-G12V (Figure 44). Other surface markers of MPN or AML cells induced by N-Ras-G12V or N-Ras-G12V and

ASXL1-MT, respectively, were similar although expression of CD11b and c-kit was slightly higher in N-Ras-G12V and ASXL1-MT-induced AML compared to N-Ras-G12V-induced MPN (Figure 45). Thus, ASXL1-MT accelerated the onset of MPN induced by N-Ras-G12V and resulted in moderate increase in immature blasts and leukemic transformation with increased expression of *Hoxa9* and decreased expression of *Clec5a*.

miR-125a is responsible for the repression of Clec5a by ASXL1-MT

As shown in Figure 35, H3K27me3, a transcriptionally repressive mark, was globally reduced by ASXL1-MT. In order to ascertain whether a microRNA (miRNA) involved in myeloid transformation might be upregulated with *ASXL1* mutations, we performed microarray analysis of miRNAs in ASXL1-MT-transduced BM cells and mock-transduced BM cells of the BMT model. We identified increased expression of several miRNAs in BM cells expressing ASXL1-MT including miR-671, miR-125a, miR-714, miR-18b, miR-129, and miR-3107. Among these, miR-125a is known to regulate hematopoietic stem cell numbers and induce MPN in a mouse BMT model (27, 73). A closely related miRNA, miR125b induces a variety of hematological

malignancies in transgenic mice and BMT models (54, 74, 75). We confirmed that expression of miR125a was increased in 32Dcl3 cells expressing ASXL1-MT when compared to those expressing ASXL1-WT or the empty vector (Figure 46). We next evaluated whether *Clec5a* is a target gene of miR125a. We identified a recognition site of miR-125a in the 3' untranslated region (UTR) of mouse *Clec5a* and two recognition sites in the 3' UTR of human *CLEC5A* (Figure 47). Therefore, we focused on mmu-miR-125a and further investigated the effects of miR-125a expression.

First, to confirm that 3'UTR of the murine *Clec5a* gene was targeted by miR125a, we generated an EF1α promoter-driven luciferase construct harboring the 3'UTR of the *Clec5a* gene (Figure 48) and performed a luciferase assay. As expected, the presence of the 3'UTR of the *Clec5a* gene reduced luciferase activity (Figure 49). This reduction was completely cancelled by mutating the miR-125a target sequence in the 3'UTR of the *Clec5a* gene (Figure 48 and 49). miR-125b1 and 2 are genes distinct from miR-125a, but their seed sequence is identical with that of miR-125a. When miR-125a or miR-125b was expressed in 32Dcl3 cells, *Clec5a* expression was reduced both at mRNA levels and surface expression levels (Figure 50 and 51) compared to 32Dcl3 cells transduced with empty vector. Moreover, these cells became more resistant to

G-CSF-induced differentiation (Figure 52). These results clearly demonstrate that miR-125a targets *Clec5a* expression, leading to the inhibition of differentiation.

We next examined H3K27me3 near the transcription start site (TSS) of miR-125a in 32Dcl3 cells transduced with the empty vector, ASXL1-MT, or ASXL1-WT. This revealed profound reduction of H3K27me3 near the TSS of miR-125a in 32Dcl3 cells expressing ASXL1-MT (Figure 53, 54, and 55). Moreover, H3K27me3 near TSS of miR-125a was also reduced in BM cells of the mice that developed MDS after the transplantation of the ASXL1-MT-transduced BM cells when compared with cells from mice engrafted with control BM cells (Figure 53, 56, and 57). Intriguingly, EZH2 binding to the miR-125a locus was reduced in ASXL1-MT-expressing 32Dcl3 cells or in ASXL1-MT-transduced BM cells from mice that developed MDS while ASXL1-WT seemed to increase EZH2 binding to the miR-125a locus (Figure 54 and 56). Altogether, these results indicated a scenario in which ASXL1-MT hampered EZH2 binding to the miR-125a locus and suppressed EZH2-mediated H3K27me3 near TSS of the miR-125a gene, leading to derepression of miR-125a, and the increased miR-125a expression inhibited the expression of *Clec5a*, contributing to the impaired differentiation of mouse BM cells which developed MDS.

Discussion

We have established and characterized a mouse MDS model induced by *ASXL1* mutations using mouse BMT model. Although MDS patients frequently harbor multiple somatic mutations, it is not clear if combinations of multiple mutations are required for the development of MDS. In addition, the molecular mechanisms of MDS pathogenesis remain elusive, particularly for recently identified mutations in epigenetic factors. Here we demonstrate that expression of the ASXL1 truncation mutant (ASXL1-MT) alone induces MDS in the mouse BMT model after a long latency, indicating that ASXL1-MT is a driver mutation in MDS development. Mutations in *ASXL1* have been reported in patients with the entire spectrum of myeloid malignancies and are recurrently associated with adverse overall survival, independent of conventional clinical predictors (43, 76), highlighting a critical need to understand the precise mechanism of transformation by *ASXL1* mutations. Recently, it was indicated that a subset of *ASXL1* mutations result in loss of stable expression of full-length *ASXL1* and that depletion of ASXL1 promoted myeloid transformation through impaired PRC2-mediated H3K27 methylation (35). On

the other hand, we demonstrated that expression of the ASXL1 truncation mutant exerts a dominant-negative role on PRC2 function. Therefore, it is important to determine whether *ASXL1* mutations exert loss-of function or gain-of-function effects. The most possible explanation of the former is that a premature stop codon may result in NMD response (64). However, it has been demonstrated that only the premature stop codon more than 50-54 nucleotides upstream of the last exon-exon junction can be a target as NMD (64). As described above, *ASXL1* mutations mostly occur as heterozygous mutations and the mutations conspicuously occur as nonsense and frameshift mutations in the last exon prior to the PHD domain, leading to escaping from NMD. Additionally, we confirmed the expression of ASXL1 transcripts even using leukemia cell lines with *ASXL1* homozygous or heterozygous mutations (Figure 7), suggesting a stable protein product which may have gain-of-function, although we found slight discrepancy between the expression levels of its transcript and its protein (Figure 6 and 7). Although a previous study reported that ASXL1 mutant protein cannot be detected by Western blotting analyses, we consider that this problem is due to lack of high-quality antibodies against N-terminus peptides and due to the protein degradation by proteasome. To determine whether ASXL1-WT and ASXL1-MT proteins express or are subject to

degradation similarly, we are now planning to produce novel antibodies against N-terminus peptides for Western blotting. By mass spectrometry, in fact, we detected several oligo-peptides of ASXL1 protein from MEG-01 cell lines with *ASXL1* homozygous mutations (G646WfsX12).

Using both *in vivo* and *in vitro* experiments, we identified that stable expression of ASXL1-MT, which inhibits the binding of ASXL1-WT to EZH2 and results in global downregulation of H3K27me3, impaired myeloid differentiation, and collaborated with co-occurring genetic alterations as was seen with downregulation of ASXL1-WT. The observation that expression of ASXL1-MT mirrors the effects of downregulation of ASXL1-WT strongly suggests that in addition to known loss-of-function mutations, a subset of *ASXL1* mutations confer a dominant-negative activity. In any case, global reduction of H3K27me3 levels has been identified both in knockdown or dominant negative model, suggesting impairing PRC2 function (35, 77). Thus, inhibiting the function of ASXL1-WT protein might lead to the similar results. In fact, a recent study reported that *Asxl1*+/- mice also developed mild MDS-like disease, demonstrating a haploinsufficient effect of *Asxl1* in the pathogenesis of myeloid malignancies (77). As mentioned in introduction, loss of function *EZH2* mutations have been identified in

some parts of MDS patients to a lesser extent compared to *ASXL1* mutations (38, 39). Interestingly, recent study reported that deletion of *EZH2* alone was enough to induce MDS/MPN-like disease in mice (78). Consequently, it may be natural to consider that ASXL1-MT and EZH2-MT, at least in part, should share the same mechanism for MDS development. However, as far as we know, *ASXL1* mutations and *EZH2* mutations are not mutually exclusive in MDS patients and ChIP analyses data of *EZH2* KO mice are quite different from those in our MDS model (38, 78), implying that ASXL1-MT may have another effect other than inhibiting EZH2. Thus, it should be elucidated whether ASXL1-MT induces characteristic DNA methylation pattern or histone modification pattern other than H3K27.

Expression of ASXL1-MT as demonstrated here resulted in impaired myeloid differentiation *in vitro* and *in vivo*. *ASXL1* mutations are most frequent in patients with MDS, MDS/MPN overlap syndromes, and in AML with myelodysplasia-related changes, highlighting a close relationship between impaired myeloid differentiation and *ASXL1* mutations (79). We identified that expression of ASXL1-MT *in vivo* results in the development of a lethal disorder characterized by morphologic dysplasia, pancytopenia, hypercellular BM and impaired myeloid differentiation with subsequent

transformation to AML in some cases, all hallmarks of human MDS. Moreover, co-expression of mutant forms of ASXL1 with oncogenic N-RAS, a complex genotype common to patients with CMML (45), results in a lethal myeloid malignancy with shorter latency than that seen with oncogenic N-RAS alone. Given the paucity of genetically-accurate murine models of MDS, expression of ASXL1-MT as demonstrated here may be quite valuable for further mechanistic and preclinical studies of MDS and AML with myelodysplasia-related changes. Interestingly, it has been recently reported that disruption of the ASXL1-interacting molecule BAP1 in mice induced CMML-like disease characterized by monocytosis and myelodysplasia (80). *BAP1* mutation was also identified in a patient with MDS, implicating the BAP1-ASXL1 axis in suppressing MDS. The contribution of disruption of the ASXL1-BAP1 axis (PRC1-related), versus loss of H3K27-trimethylation (PRC2-related), in promoting myeloid transformation induced by ASXL1-MT requires further evaluation.

To understand the transcriptional events responsible for the biological effects of *ASXL1* mutations in more detail, we performed transcriptomic studies in the presence of mutant ASXL1 *in vitro* and *in vivo*. In addition to identifying significant upregulation of

posterior *Hoxa* genes, we identified increased expression of miR-125a due to locus-specific downregulation of H3K27 methylation. Moreover, it has been reported that miR-125a is upregulated after inhibition of *EZH2* by knockdown in DU145 prostate cancer cells (81). miR-125a was the only miR upregulated in both our murine system and in primary human MDS samples (82). miR-125a belongs to a microRNA family including miR-125a, miR-125b-1 and miR-125b-2, all of which have the same seed sequence and have been implicated in human leukemia/lymphoma (83-85) as well as in MDS (82). Forced expression of these miRs has been previously shown to induce the expansion of hemopoietic stem cells or hamper myeloid differentiation (27, 54, 73, 74, 82, 85)

Although several proapoptotic genes have been implicated for hematopoietic transformation as miR-125a targets (27, 54, 86), here we identified direct repression of a novel target *Clec5a* by miR-125a as a specific effector of the differentiation phenotype. The type II membrane protein CLEC5A belongs to the lectin family is a receptor for Dengue virus on the surface of macrophages and result in the release of proinflammatory cytokines through adaptor protein DAP12 pathway (69). However, as far as we know, the endogenous ligand has not been identified. Previously, it has been

recognized that *Clec5a* expression is correlated with myeloid differentiation as *Clec5a* is expressed in monocytes and neutrophils, and its expression is increased by granulocytic differentiation of 32Dcl3 cells (70) and monocytic differentiation of U937 cells and primary progenitor cells (87). Here, we present clear evidence that *Clec5a* supports myeloid differentiation. First, ASXL1-MT but not ASXL1-WT reduced expression of *Clec5a* in 32Dcl3 cells and impaired G-CSF-induced granulocytic differentiation. Second, in 32Dcl3 cells expressing ASXL1-MT, myeloid differentiation was partly restored by the forced expression of Clec5a but not by a mutant Clec5a (Clec5a-K16A) which cannot associate with DAP12. Third, knockdown of *Clec5a* impaired G-CSF-induced differentiation of 32Dcl3 cells. In addition, *Clec5a* expression was downregulated in the ASXL1-MT-induced MDS mice. These results indicate that downregulation of *Clec5a* by ASXL1-MT impairs myeloid differentiation and is involved in MDS development. Interestingly, *w*hile *HOXA9* expression was high in MDS patients with *ASXL1* mutations (Figure 37), the expression level of *CLEC5A* was generally low in MDS patients compared with controls and did not correlate with the presence of *ASXL1* mutations (Figure 23). This suggests that *CLEC5A* expression is reduced in MDS by multiple causes including *ASXL1* mutations, and that reduction of

CLEC5A might play a general role in the pathogenesis of MDS. Prior data indicating downregulation of *CLEC5A* expression in acute leukemia likewise supports the possibility that *CLEC5A* downregulation may be important in the pathogenesis of multiple subtypes of myeloid malignancies (88).

The data presented here indicate that *ASXL1* mutations which result in a truncated protein product may (1) inhibit PRC2-function in a dominant-negative fashion and (2) promote myeloid transformation through impaired PRC2-mediated repression of posterior *HOXA*s and miR-125a, and subsequent miR-125a-supression of *CLEC5A*. Thus, although changes in expression of other genes caused by *ASXL1* mutations may also be involved, it is documented that the derepression of *HOXA*s and miR-125a and the suppression of *CLEC5A* contribute to the development of MDS (Figure 58). Given the clinical importance of *ASXL1* mutations, the identification of gain-of-function *ASXL1* mutations is critical as it provides a rationale for therapies aimed at targeting the expressed mutant forms of ASXL1. Finally, the data here provides further basis for the involvement of miR-125 in myeloid malignancy pathogenesis and identify an important role for *CLEC5A* in the pathogenesis of multiple genetic subtypes of myeloid malignancies.

Acknowledgements

I would like to sincerely thank my supervisor Prof. Toshio Kitamura for his educational support in his laboratory. His mentorship was paramount in training to be an independent scientist. I am also grateful to Dr. Jiro Kitaura for his helpful advice on my research. In addition, I would like to thank Dr. Tomoyuki Uchida for his technical advice and Dr. Katsuhiro Togami for date analysis. And this study is based on the discussion with many outstanding researchers. I thank Dr. Omar Abdel-Wahab (Memorial Sloan-Kettering Cancer Center, USA), Dr. Ross L. Levine (Memorial Sloan-Kettering Cancer Center, USA), Dr. Atsushi Iwama (Chiba University), Dr. Makoto Nakanishi (Nagoya City University), Dr. Hiroyuki Aburatani (The University of Tokyo), Dr. Shogo Yamamoto (The University of Tokyo), and Dr. Koutarou Nishimura (The University of Tokyo) for their helpful discussions. Also, I was blessed with many researchers who were ready to give me human samples and antibodies. Especially, I would like to thank Dr. Hiroshi Kimura (Osaka University), Dr. Yuka Harada (Juntendo University), Dr. Hironori Harada (Juntendo University), Dr. Felicitas Thol (Hannover Medical School, Germany), Dr. Michael Heuser (Hannover Medical School, Germany)

and Dr. Omar Abdel-Wahab. Lastly, I would like to show my gratitude to my wife and all my family members for their love and support.

References

1. Portela A, and Esteller M. Epigenetic modifications and human disease. *Nat Biotechnol.* 2010;28(10):1057-68.

2. Dawson MA, and Kouzarides T. Cancer epigenetics: from mechanism to therapy. *Cell.* 2012;150(1):12-27.

3. Ballestar E, and Esteller M. Epigenetic gene regulation in cancer. *Adv Genet.* 2008;61:247-67.

4. Esteller M. Epigenetics in cancer. *N Engl J Med.* 2008;358(11):1148-59.

5. Carmona FJ, and Esteller M. Epigenomics of human colon cancer. *Mutat Res.* 2010;693(1-2):53-60.

6. Veeck J, and Esteller M. Breast cancer epigenetics: from DNA methylation to microRNAs. *J Mammary Gland Biol Neoplasia.* 2010;15(1):5-17.

7. Vendetti FP, and Rudin CM. Epigenetic therapy in non-small-cell lung cancer: targeting DNA methyltransferases and histone deacetylases. *Expert Opin Biol Ther.* 2013;13(9):1273-85.

8. Sandoval J, and Esteller M. Cancer epigenomics: beyond genomics. *Curr Opin Genet Dev.* 2012;22(1):50-5.

9. Issa JP. The myelodysplastic syndrome as a prototypical epigenetic disease. *Blood.* 2013;121(19):3811-7.

10. Esteller M. Profiling aberrant DNA methylation in hematologic neoplasms: a view from the tip of the iceberg. *Clin Immunol.* 2003;109(1):80-8.

11. Read CM, Baldwin JP, and Crane-Robinson C. Structure of subnucleosomal particles. Tetrameric (H3/H4)2 146 base pair DNA and hexameric (H3/H4)2(H2A/H2B)1 146 base pair DNA complexes. *Biochemistry.* 1985;24(16):4435-50.

12. Thompson LL, Guppy BJ, Sawchuk L, Davie JR, and McManus KJ. Regulation of chromatin structure via histone post-translational modification and the link to carcinogenesis. *Cancer Metastasis Rev.* 2013;32(3-4):363-76.

13. Vasudevan D, Chua EY, and Davey CA. Crystal structures of nucleosome core particles containing the '601' strong positioning sequence. *J Mol Biol.* 2010;403(1):1-10.

14. Esteller M. Cancer epigenomics: DNA methylomes and histone-modification maps. *Nat Rev Genet.* 2007;8(4):286-98.

15. Rice KL, Hormaeche I, and Licht JD. Epigenetic regulation of normal and malignant hematopoiesis. *Oncogene.* 2007;26(47):6697-714.

16. Chi P, Allis CD, and Wang GG. Covalent histone modifications--miswritten, misinterpreted and mis-erased in human cancers. *Nat Rev Cancer.* 2010;10(7):457-69.

17. Bannister AJ, and Kouzarides T. Regulation of chromatin by histone modifications. *Cell Res.* 2011;21(3):381-95.

18. Strahl BD, and Allis CD. The language of covalent histone modifications. *Nature.* 2000;403(6765):41-5.

19. Jenuwein T, and Allis CD. Translating the histone code. *Science.* 2001;293(5532):1074-80.

20. Cosgrove MS. Writers and readers: deconvoluting the harmonic complexity of the histone code. *Nat Struct Mol Biol.* 2012;19(8):739-40.

21. Sinclair DA, Campbell RB, Nicholls F, Slade E, and Brock HW.

Genetic analysis of the additional sex combs locus of Drosophila melanogaster. *Genetics.* 1992;130(4):817-25.

22. Milne TA, Sinclair DA, and Brock HW. The Additional sex combs gene of Drosophila is required for activation and repression of homeotic loci, and interacts specifically with Polycomb and super sex combs. *Mol Gen Genet.* 1999;261(4-5):753-61.

23. Campbell RB, Sinclair DA, Couling M, and Brock HW. Genetic interactions and dosage effects of Polycomb group genes of Drosophila. *Mol Gen Genet.* 1995;246(3):291-300.

24. Fisher CL, Lee I, Bloyer S, Bozza S, Chevalier J, Dahl A, Bodner C, Helgason CD, Hess JL, Humphries RK, et al. Additional sex combs-like 1 belongs to the enhancer of trithorax and polycomb group and genetically interacts with Cbx2 in mice. *Dev Biol.* 2010;337(1):9-15.

25. Park UH, Yoon SK, Park T, Kim EJ, and Um SJ. Additional sex comb-like (ASXL) proteins 1 and 2 play opposite roles in adipogenesis via reciprocal regulation of peroxisome proliferator-activated receptor {gamma}. *J Biol Chem.* 2011;286(2):1354-63.

26. Cho YS, Kim EJ, Park UH, Sin HS, and Um SJ. Additional sex comb-like 1 (ASXL1), in cooperation with SRC-1, acts as a ligand-dependent coactivator for retinoic acid receptor. *J Biol Chem.* 2006;281(26):17588-98.

27. Guo S, Bai H, Megyola CM, Halene S, Krause DS, Scadden DT, and Lu J. Complex oncogene dependence in microRNA-125a-induced myeloproliferative neoplasms. *Proc Natl Acad Sci U S A.* 2012;109(41):16636-41.

28. Hoischen A, van Bon BW, Rodríguez-Santiago B, Gilissen C, Vissers LE, de Vries P, Janssen I, van Lier B, Hastings R, Smithson SF, et al. De novo nonsense mutations in ASXL1 cause Bohring-Opitz syndrome.

Nat Genet. 2011;43(8):729-31.

29. Fisher CL, Randazzo F, Humphries RK, and Brock HW. Characterization of Asxl1, a murine homolog of Additional sex combs, and analysis of the Asx-like gene family. *Gene.* 2006;369:109-18.

30. Scheuermann JC, de Ayala Alonso AG, Oktaba K, Ly-Hartig N, McGinty RK, Fraterman S, Wilm M, Muir TW, and Müller J. Histone H2A deubiquitinase activity of the Polycomb repressive complex PR-DUB. *Nature.* 2010;465(7295):243-7.

31. Lee SW, Cho YS, Na JM, Park UH, Kang M, Kim EJ, and Um SJ. ASXL1 represses retinoic acid receptor-mediated transcription through associating with HP1 and LSD1. *J Biol Chem.* 2010;285(1):18-29.

32. Rosenfeld MG, and Glass CK. Coregulator codes of transcriptional regulation by nuclear receptors. *J Biol Chem.* 2001;276(40):36865-8.

33. Liu L, Qin S, Zhang J, Ji P, Shi Y, and Wu J. Solution structure of an atypical PHD finger in BRPF2 and its interaction with DNA. *J Struct Biol.* 2012;180(1):165-73.

34. Sanchez-Pulido L, Kong L, and Ponting CP. A common ancestry for BAP1 and Uch37 regulators. *Bioinformatics.* 2012;28(15):1953-6.

35. Abdel-Wahab O, Adli M, LaFave LM, Gao J, Hricik T, Shih AH, Pandey S, Patel JP, Chung YR, Koche R, et al. ASXL1 mutations promote myeloid transformation through loss of PRC2-mediated gene repression. *Cancer Cell.* 2012;22(2):180-93.

36. Scheuermann JC, de Ayala Alonso AG, Oktaba K, Ly-Hartig N, McGinty RK, Fraterman S, Wilm M, Muir TW, and Muller J. Histone H2A deubiquitinase activity of the Polycomb repressive complex PR-DUB. *Nature.* 2010;465(7295):243-7.

37. Chung YR, Schatoff E, and Abdel-Wahab O. Epigenetic alterations in

hematopoietic malignancies. *Int J Hematol.* 2012;96(4):413-27.

38. Abdel-Wahab O, and Figueroa ME. Interpreting new molecular genetics in myelodysplastic syndromes. *Hematology Am Soc Hematol Educ Program.* 2012;2012:56-64.

39. Graubert T, and Walter MJ. Genetics of myelodysplastic syndromes: new insights. *Hematology Am Soc Hematol Educ Program.* 2011;2011:543-9.

40. Rocquain J, Carbuccia N, Trouplin V, Raynaud S, Murati A, Nezri M, Tadrist Z, Olschwang S, Vey N, Birnbaum D, et al. Combined mutations of ASXL1, CBL, FLT3, IDH1, IDH2, JAK2, KRAS, NPM1, NRAS, RUNX1, TET2 and WT1 genes in myelodysplastic syndromes and acute myeloid leukemias. *BMC Cancer*. 2010;10:401.

41. Gelsi-Boyer V, Trouplin V, Adelaide J, Bonansea J, Cervera N, Carbuccia N, Lagarde A, Prebet T, Nezri M, Sainty D, et al. Mutations of polycomb-associated gene ASXL1 in myelodysplastic syndromes and chronic myelomonocytic leukaemia. *Br J Haematol.* 2009;145(6):788-800.

42. Boultwood J, Perry J, Pellagatti A, Fernandez-Mercado M, Fernandez-Santamaria C, Calasanz MJ, Larrayoz MJ, Garcia-Delgado M, Giagounidis A, Malcovati L, et al. Frequent mutation of the polycomb-associated gene ASXL1 in the myelodysplastic syndromes and in acute myeloid leukemia. *Leukemia.* 2010;24(5):1062-5.

43. Thol F, Friesen I, Damm F, Yun H, Weissinger EM, Krauter J, Wagner K, Chaturvedi A, Sharma A, Wichmann M, et al. Prognostic significance of ASXL1 mutations in patients with myelodysplastic syndromes. *J Clin Oncol.* 2011;29(18):2499-506.

44. Gelsi-Boyer V, Trouplin V, Roquain J, Adelaide J, Carbuccia N, Esterni B, Finetti P, Murati A, Arnoulet C, Zerazhi H, et al. ASXL1 mutation

is associated with poor prognosis and acute transformation in chronic myelomonocytic leukaemia. *Br J Haematol.* 2010;151(4):365-75.

45. Abdel-Wahab O, Pardanani A, Patel J, Wadleigh M, Lasho T, Heguy A, Beran M, Gilliland DG, Levine RL, and Tefferi A. Concomitant analysis of EZH2 and ASXL1 mutations in myelofibrosis, chronic myelomonocytic leukemia and blast-phase myeloproliferative neoplasms. *Leukemia.* 2011;25(7):1200-2.

46. Garcia-Manero G. Prognosis of myelodysplastic syndromes. *Hematology Am Soc Hematol Educ Program.* 2010;2010:330-7.

47. Nimer SD. MDS: a stem cell disorder--but what exactly is wrong with the primitive hematopoietic cells in this disease? *Hematology Am Soc Hematol Educ Program.* 2008:43-51.

48. Deeg HJ. Optimization of transplant regimens for patients with myelodysplastic syndrome (MDS). *Hematology Am Soc Hematol Educ Program.* 2005:167-73.

49. Santini V. Novel therapeutic strategies: hypomethylating agents and beyond. *Hematology Am Soc Hematol Educ Program.* 2012;2012:65-73.

50. Adès L, and Fenaux P. Immunomodulating drugs in myelodysplastic syndromes. *Hematology Am Soc Hematol Educ Program.* 2011;2011:556-60.

51. Nikoloski G, van der Reijden BA, and Jansen JH. Mutations in epigenetic regulators in myelodysplastic syndromes. *Int J Hematol.* 2012;95(1):8-16.

52. Vainchenker W, Delhommeau F, Constantinescu SN, and Bernard OA. New mutations and pathogenesis of myeloproliferative neoplasms. *Blood.* 2011;118(7):1723-35.

53. Kitamura T, Koshino Y, Shibata F, Oki T, Nakajima H, Nosaka T, and

Kumagai H. Retrovirus-mediated gene transfer and expression cloning: powerful tools in functional genomics. *Exp Hematol.* 2003;31(11):1007-14.

54. Enomoto Y, Kitaura J, Hatakeyama K, Watanuki J, Akasaka T, Kato N, Shimanuki M, Nishimura K, Takahashi M, Taniwaki M, et al. Emu/miR-125b transgenic mice develop lethal B-cell malignancies. *Leukemia.* 2011;25(12):1849-56.

55. Watanabe-Okochi N, Kitaura J, Ono R, Harada H, Harada Y, Komeno Y, Nakajima H, Nosaka T, Inaba T, and Kitamura T. AML1 mutations induced MDS and MDS/AML in a mouse BMT model. *Blood.* 2008;111(8):4297-308.

56. Enomoto Y, Yamanishi Y, Izawa K, Kaitani A, Takahashi M, Maehara A, Oki T, Takamatsu R, Kajikawa M, Takai T, et al. Characterization of leukocyte mono-immunoglobulin-like receptor 7 (LMIR7)/CLM-3 as an activating receptor: its similarities to and differences from LMIR4/CLM-5. *J Biol Chem.* 2010;285(46):35274-83.

57. Ono R, Nakajima H, Ozaki K, Kumagai H, Kawashima T, Taki T, Kitamura T, Hayashi Y, and Nosaka T. Dimerization of MLL fusion proteins and FLT3 activation synergize to induce multiple-lineage leukemogenesis. *J Clin Invest.* 2005;115(4):919-29.

58. Kimura H, Hayashi-Takanaka Y, Goto Y, Takizawa N, and Nozaki N. The organization of histone H3 modifications as revealed by a panel of specific monoclonal antibodies. *Cell Struct Funct.* 2008;33(1):61-73.

59. Nozawa RS, Nagao K, Masuda HT, Iwasaki O, Hirota T, Nozaki N, Kimura H, and Obuse C. Human POGZ modulates dissociation of HP1alpha from mitotic chromosome arms through Aurora B activation. *Nat Cell Biol.* 2010;12(7):719-27.

60. Tanaka S, Miyagi S, Sashida G, Chiba T, Yuan J, Mochizuki-Kashio M, Suzuki Y, Sugano S, Nakaseko C, Yokote K, et al. Ezh2 augments

leukemogenicity by reinforcing differentiation blockage in acute myeloid leukemia. *Blood.* 2012;120(5):1107-17.

61. Kato N, Kitaura J, Doki N, Komeno Y, Watanabe-Okochi N, Togami K, Nakahara F, Oki T, Enomoto Y, Fukuchi Y, et al. Two types of C/EBPα mutations play distinct but collaborative roles in leukemogenesis: lessons from clinical data and BMT models. *Blood.* 2011;117(1):221-33.

62. Piazza F, Valens J, Lagasse E, and Schindler C. Myeloid differentiation of FdCP1 cells is dependent on Stat5 processing. *Blood.* 2000;96(4):1358-65.

63. Subramanian A, Tamayo P, Mootha VK, Mukherjee S, Ebert BL, Gillette MA, Paulovich A, Pomeroy SL, Golub TR, Lander ES, et al. Gene set enrichment analysis: a knowledge-based approach for interpreting genome-wide expression profiles. *Proc Natl Acad Sci U S A.* 2005;102(43):15545-50.

64. Maquat LE. Nonsense-mediated mRNA decay in mammals. *J Cell Sci.* 2005;118(Pt 9):1773-6.

65. Abdel-Wahab O, Kilpivaara O, Patel J, Busque L, and Levine RL. The most commonly reported variant in ASXL1 (c.1934dupG;p.Gly646TrpfsX12) is not a somatic alteration. *Leukemia.* 2010;24(9):1656-7.

66. Schnittger S, Eder C, Jeromin S, Alpermann T, Fasan A, Grossmann V, Kohlmann A, Illig T, Klopp N, Wichmann HE, et al. ASXL1 exon 12 mutations are frequent in AML with intermediate risk karyotype and are independently associated with an adverse outcome. *Leukemia.* 2013;27(1):82-91.

67. Schlegelberger B, Gohring G, Thol F, and Heuser M. Update on cytogenetic and molecular changes in myelodysplastic syndromes. *Leuk Lymphoma.* 2012;53(4):525-36.

68. Gelsi-Boyer V, Brecqueville M, Devillier R, Murati A, Mozziconacci MJ, and Birnbaum D. Mutations in ASXL1 are associated with poor prognosis across the spectrum of malignant myeloid diseases. *J Hematol Oncol.* 2012;5:12.

69. Bakker AB, Baker E, Sutherland GR, Phillips JH, and Lanier LL. Myeloid DAP12-associating lectin (MDL)-1 is a cell surface receptor involved in the activation of myeloid cells. *Proc Natl Acad Sci U S A.* 1999;96(17):9792-6.

70. Aoki N, Kimura Y, Kimura S, Nagato T, Azumi M, Kobayashi H, Sato K, and Tateno M. Expression and functional role of MDL-1 (CLEC5A) in mouse myeloid lineage cells. *J Leukoc Biol.* 2009;85(3):508-17.

71. Kim J, Woo AJ, Chu J, Snow JW, Fujiwara Y, Kim CG, Cantor AB, and Orkin SH. A Myc network accounts for similarities between embryonic stem and cancer cell transcription programs. *Cell.* 2010;143(2):313-24.

72. MacKenzie KL, Dolnikov A, Millington M, Shounan Y, and Symonds G. Mutant N-ras induces myeloproliferative disorders and apoptosis in bone marrow repopulated mice. *Blood.* 1999;93(6):2043-56.

73. Gerrits A, Walasek MA, Olthof S, Weersing E, Ritsema M, Zwart E, van Os R, Bystrykh LV, and de Haan G. Genetic screen identifies microRNA cluster 99b/let-7e/125a as a regulator of primitive hematopoietic cells. *Blood.* 2012;119(2):377-87.

74. Chaudhuri AA, So AY, Mehta A, Minisandram A, Sinha N, Jonsson VD, Rao DS, O'Connell RM, and Baltimore D. Oncomir miR-125b regulates hematopoiesis by targeting the gene Lin28A. *Proc Natl Acad Sci U S A.* 2012;109(11):4233-8.

75. Bousquet M, Harris MH, Zhou B, and Lodish HF. MicroRNA miR-125b causes leukemia. *Proc Natl Acad Sci U S A.* 2010;107(50):21558-63.

76. Abdel-Wahab O, Patel J, and Levine RL. Clinical implications of novel

mutations in epigenetic modifiers in AML. *Hematol Oncol Clin North Am.* 2011;25(6):1119-33.

77. Wang J, Li Z, He Y, Pan F, Chen S, Rhodes S, Nguyen L, Yuan J, Jiang L, Yang X, et al. Loss of Asxl1 leads to myelodysplastic syndrome-like disease in mice. *Blood.* 2013; in press.

78. Muto T, Sashida G, Oshima M, Wendt GR, Mochizuki-Kashio M, Nagata Y, Sanada M, Miyagi S, Saraya A, Kamio A, et al. Concurrent loss of Ezh2 and Tet2 cooperates in the pathogenesis of myelodysplastic disorders. *J Exp Med.* 2013;210(12):2627-39.

79. Devillier R, Gelsi-Boyer V, Brecqueville M, Carbuccia N, Murati A, Vey N, Birnbaum D, and Mozziconacci MJ. Acute myeloid leukemia with myelodysplasia-related changes are characterized by a specific molecular pattern with high frequency of ASXL1 mutations. *Am J Hematol.* 2012;87(7):659-62.

80. Dey A, Seshasayee D, Noubade R, French DM, Liu J, Chaurushiya MS, Kirkpatrick DS, Pham VC, Lill JR, Bakalarski CE, et al. Loss of the tumor suppressor BAP1 causes myeloid transformation. *Science.* 2012;337(6101):1541-6.

81. Cao Q, Mani RS, Ateeq B, Dhanasekaran SM, Asangani IA, Prensner JR, Kim JH, Brenner JC, Jing X, Cao X, et al. Coordinated regulation of polycomb group complexes through microRNAs in cancer. *Cancer Cell.* 2011;20(2):187-99.

82. Rhyasen GW, and Starczynowski DT. Deregulation of microRNAs in myelodysplastic syndrome. *Leukemia.* 2012;26(1):13-22.

83. Tassano E, Acquila M, Tavella E, Micalizzi C, Panarello C, and Morerio C. MicroRNA-125b-1 and BLID upregulation resulting from a novel IGH translocation in childhood B-Cell precursor acute lymphoblastic leukemia. *Genes Chromosomes Cancer.* 2010;49(8):682-7.

84. Chapiro E, Russell LJ, Struski S, Cave H, Radford-Weiss I, Valle VD, Lachenaud J, Brousset P, Bernard OA, Harrison CJ, et al. A new recurrent translocation t(11;14)(q24;q32) involving IGH@ and miR-125b-1 in B-cell progenitor acute lymphoblastic leukemia. *Leukemia.* 2010;24(7):1362-4.

85. Bousquet M, Quelen C, Rosati R, Mansat-De Mas V, La Starza R, Bastard C, Lippert E, Talmant P, Lafage-Pochitaloff M, Leroux D, et al. Myeloid cell differentiation arrest by miR-125b-1 in myelodysplastic syndrome and acute myeloid leukemia with the t(2;11)(p21;q23) translocation. *J Exp Med.* 2008;205(11):2499-506.

86. Ooi AG, Sahoo D, Adorno M, Wang Y, Weissman IL, and Park CY. MicroRNA-125b expands hematopoietic stem cells and enriches for the lymphoid-balanced and lymphoid-biased subsets. *Proc Natl Acad Sci U S A.* 2010;107(50):21505-10.

87. Gingras MC, Lapillonne H, and Margolin JF. TREM-1, MDL-1, and DAP12 expression is associated with a mature stage of myeloid development. *Mol Immunol.* 2002;38(11):817-24.

88. Batliner J, Mancarelli MM, Jenal M, Reddy VA, Fey MF, Torbett BE, and Tschan MP. CLEC5A (MDL-1) is a novel PU.1 transcriptional target during myeloid differentiation. *Mol Immunol.* 2011;48(4):714-9.

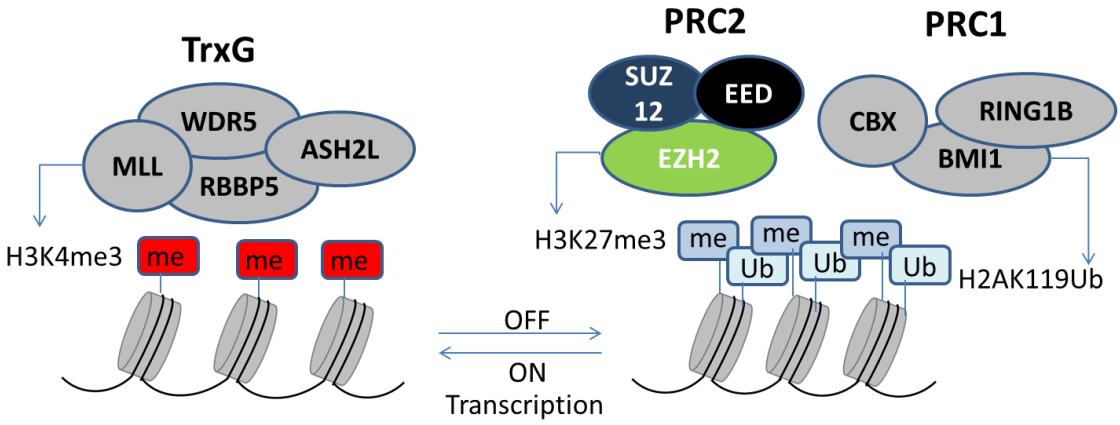

Figure 1. Schematic image of histone modifications related to gene expression. H3K4me3 is a representative active mark mediated by Trithorax group (TrxG), which is composed of MLL, WDR5, RBBP5, and ASH2L. On the other hand, H3K27me3 and H2AK119Ub are repressive marks, mediated by PRC2 and PRC1, respectively; MLL, myeloid/lymphoid or mixed-lineage leukemia; WDR5, WD repeat domain 5; RBBP5, retinoblastoma binding protein 5; ASH2L, ash2 (absent, small, or homeotic)-like; EZH2, enhancer of zeste homolog 2; SUZ12, SUZ12 polycomb repressive complex 2 subunit; EED, embryonic ectoderm development; BMI1, BMI1 polycomb ring finger oncogene; CBX, chromobox homolog; RING1B, ring finger protein 1B.

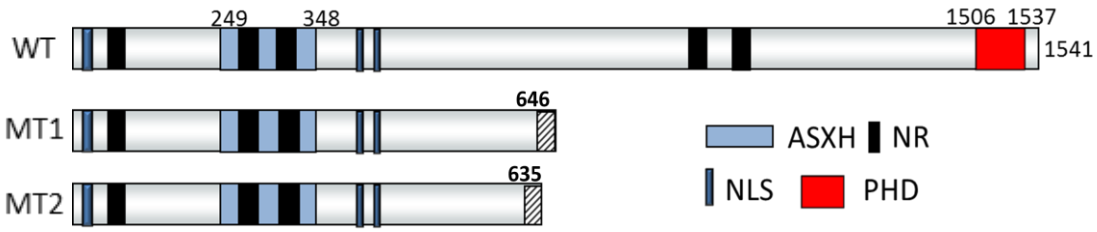

Figure 2. Schematic diagram of ASXL1-WT and two mutants, MT1 and MT2. ASXH indicates ASX homology region; NR, putative nuclear receptor coregulator binding motifs; NLS, nuclear localization signal; PHD, plant homeodomain.

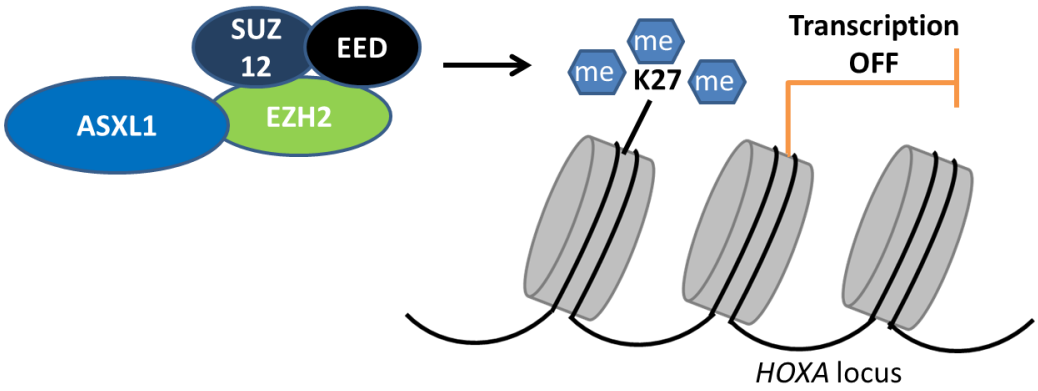

Figure 3. Schematic image of ASXL1 protein function. ASXL1-WT proteins bind to EZH2 and support PRC2 function to repress transcription in *HOXA* locus.

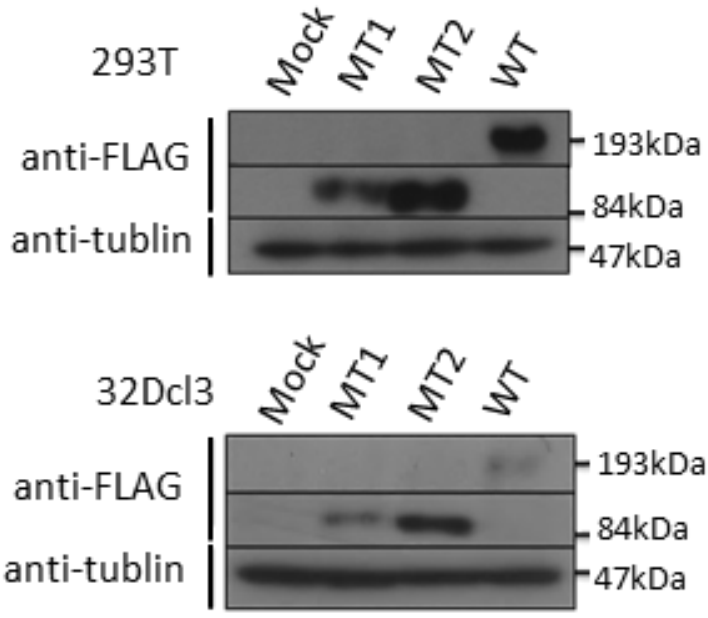

Figure 4. Expression of ASXL1-WT and its mutants in HEK293T cells or 32Dcl3 cells transiently transfected or stably transduced with a FLAG-tagged-ASXL1-MT1, ASXL1-MT2, ASXL1-WT or an empty vector (pMYs-IG), respectively.

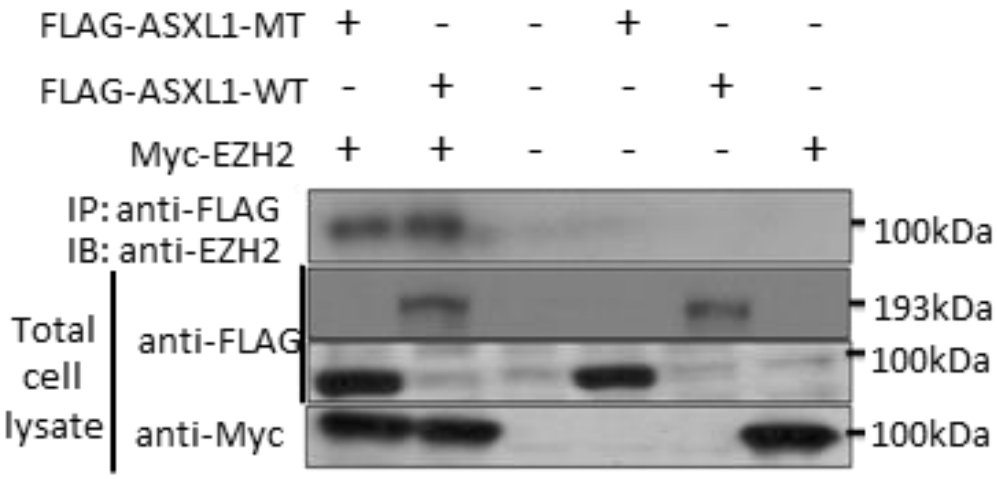

Figure 5. HEK293T cells were transiently transfected with FLAG-ASXL1-MT, FLAG-ASXL1-WT, and Myc-EZH2 cDNA as described, followed by IP of FLAG epitope and Western blotting for EZH2. Cell lysates were also subject to immunoblotting with anti-FLAG Ab or anti-Myc Ab.

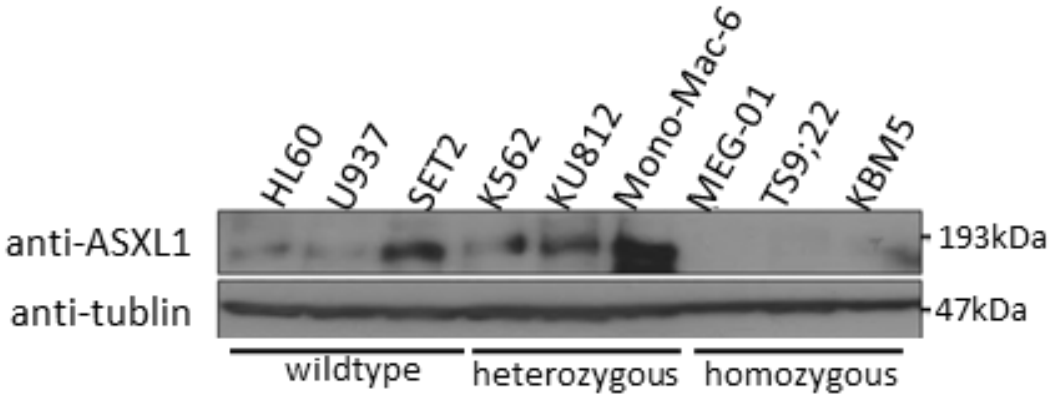

Figure 6. ASXL1 protein expression using C-terminus anti-ASXL1 antibodies in leukemia cell lines. Harboring mutations are as follows: K562, heterozygous *ASXL1* Y591Y/X; KU812, heterozygous *ASXL1* R693R/X; Mono-Mac-6, heterozygous *ASXL1* L1393RfsX30; MEG-01, homozygous *ASXL1* G646WfsX12; TS9;22, homozygous *ASXL1* R693X; KBM5 homozygous *ASXL1* G710X.

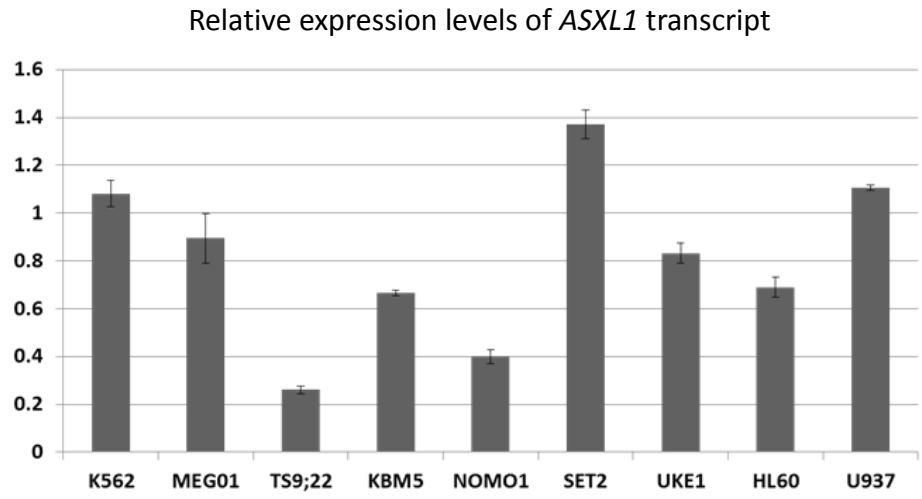

Figure 7. *ASXL1* transcript was detected in human leukemia cell lines with or without *ASXL1* mutations. Relative expression levels of *ASXL1* were examined by qRT-PCR in leukemia cell lines. *ASXL1* genes of these cell lines harbor mutations as follows: K562, heterozygous *ASXL1* Y591Y/X; MEG-01, homozygous *ASXL1* G646WfsX12; TS9;22, homozygous *ASXL1* R693X; KBM5 homozygous *ASXL1* G710X; NOMO1 homozygous *ASXL1* R639X. The values were normalized by GAPDH mRNA levels. All data with error bars are presented as mean ± SEM of two independent experiments.

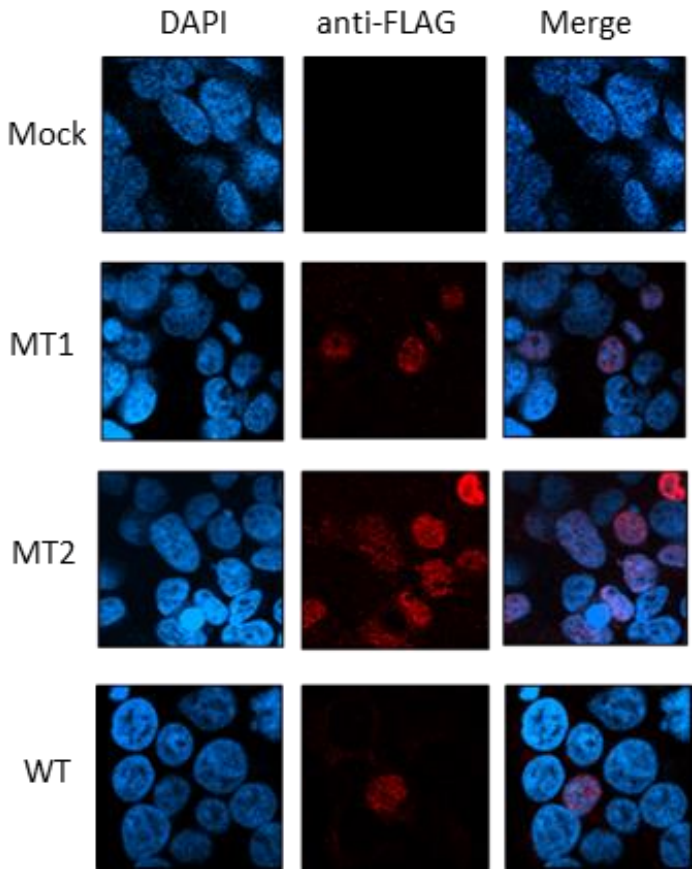

Figure 8. Nuclear localization of ASXL1-MTs. HEK293T cells transiently transfected with pMYs-IG, pMYs-FLAG-tagged-ASXL1-MT1-IG, pMYs-FLAG-tagged-ASXL1-MT2-IG, or pMYs-FLAG-tagged-ASXL1-WT-IG were immunostained with anti-FLAG Ab (red) and DAPI (blue). Original magnification, ×600.

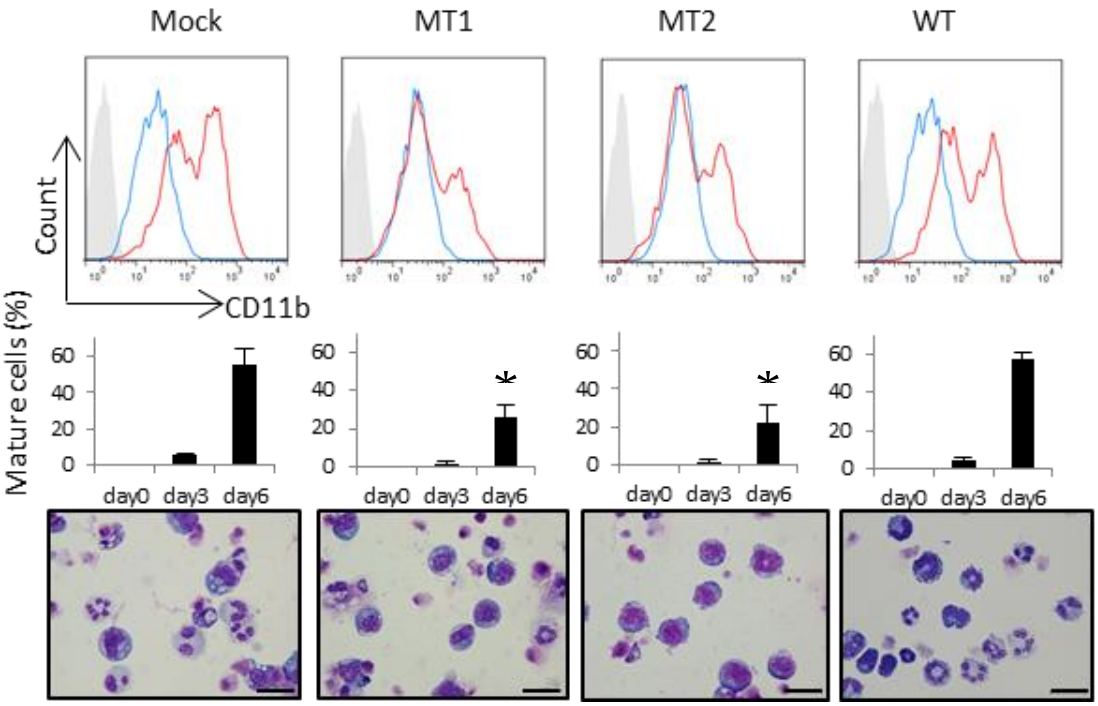

Figure 9. Surface expression of CD11b in 32Dcl3 cells transduced with indicated plasmid after incubation with 1 ng/mL IL-3 (blue) or 50 ng/mL G-CSF for six days (red) was analyzed by flow cytometry (top). Filled histograms show control (IgG). Proportion of segmented cells on day 0, 3, and 6 of G-CSF stimulation was shown (middle). Morphology of the cells six days after G-CSF stimulation was assessed by Wright-Giemsa staining (bottom). Original magnification, ×400; bars, 20 μm. *P < 0.05, compared to the proportion of mature cells in 32Dcl3 cells transduced with empty vector.

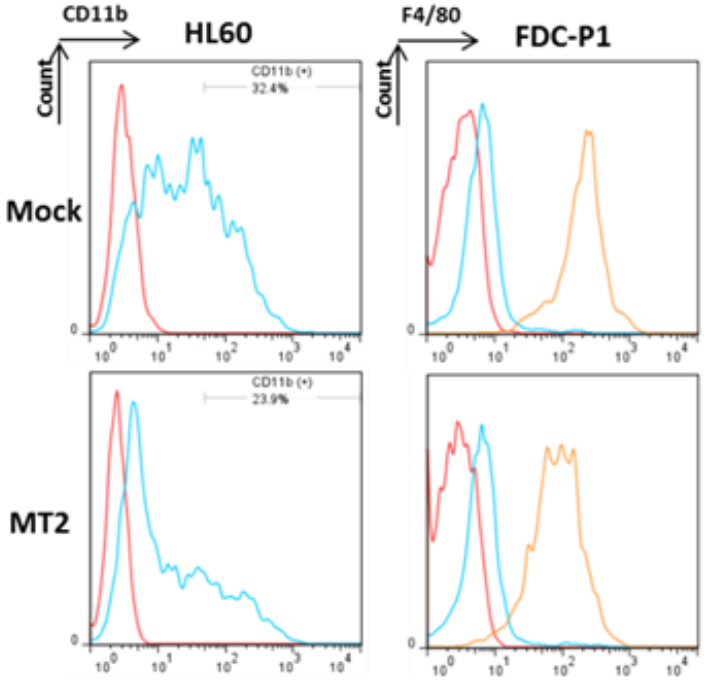

Figure 10. Surface expression of CD11b in HL60 or FDC-P1 transduced with the indicated plasmid after incubation with 10^{-6}M ATRA (left) or 10 ng/mL GM-CSF (right), respectively, for three or six days was analyzed by flow cytometry. Red histograms indicate control (IgG). (left) blue, day3; (right) blue, day3; orange, day6.

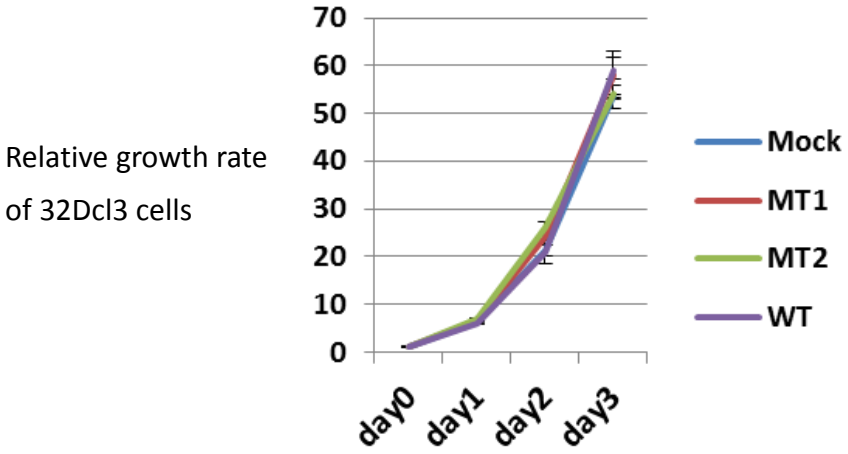

Figure 11. The relative growth rate of 32Dcl3 cells transduced with pMYs-IG (Mock), pMYs-FLAG–tagged ASXL1-MT1-IG (MT1), pMYs-FLAG–tagged ASXL1-MT2-IG (MT2), or pMYs-FLAG–tagged ASXL1-WT-IG (WT) in the presence of 1 ng/mL IL-3 (mean ± SEM).

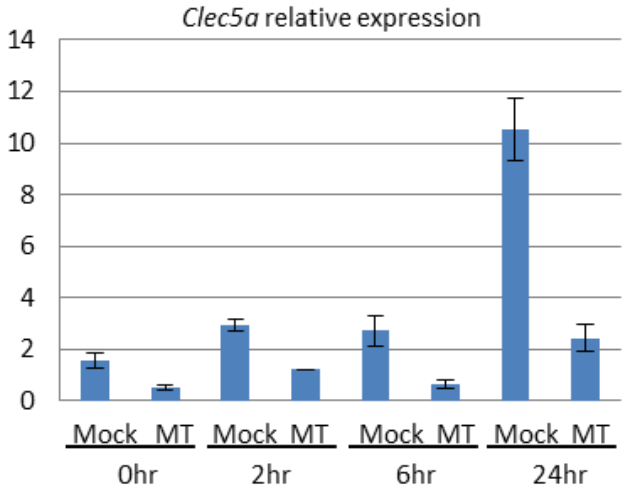

Figure 12. *ASXL1* mutations reduced the expression of *Clec5a*. qRT-PCR for *Clec5a* in 32Dcl3 cells transduced with pMYs-IG (Mock) or pMYs-FLAG-tagged-ASXL1-MT2-IG (MT). Relative expression levels normalized by *Gapdh* mRNA were measured at indicated time points after incubation with G-CSF (50 ng/ml).

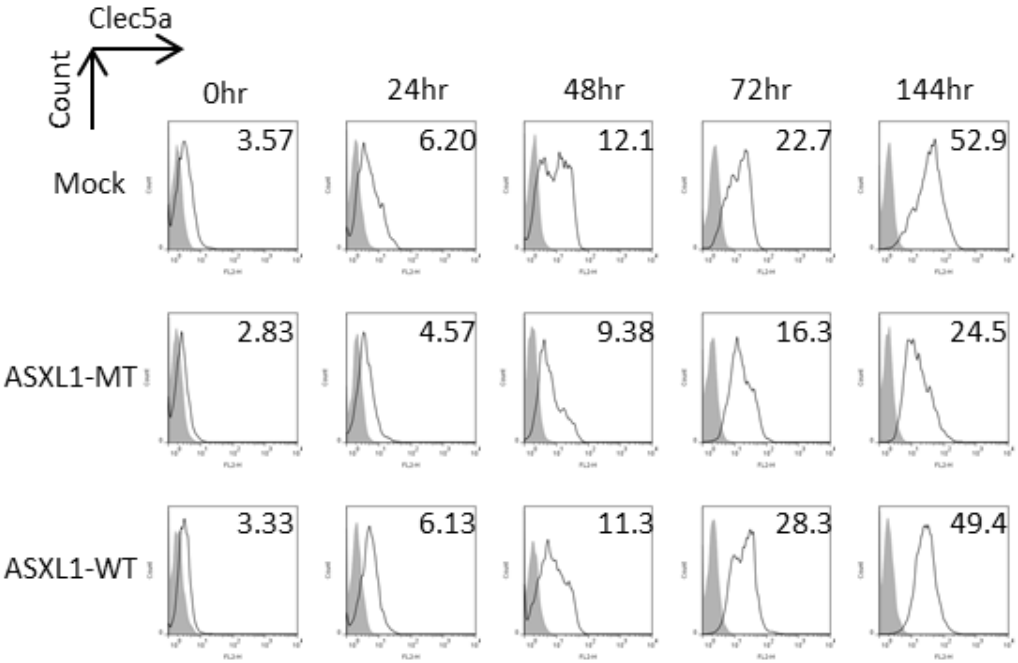

Figure 13. Surface expression of Clec5a in 32Dcl3 cells transduced with mock, ASXL1-MT2 (MT), or ASXL1-WT after incubation with 50 ng/ml G-CSF. Cells were analyzed by flow cytometry at indicated time points. Mean fluorescence intensities (MFIs) were indicated. Filled histograms show control (IgG).

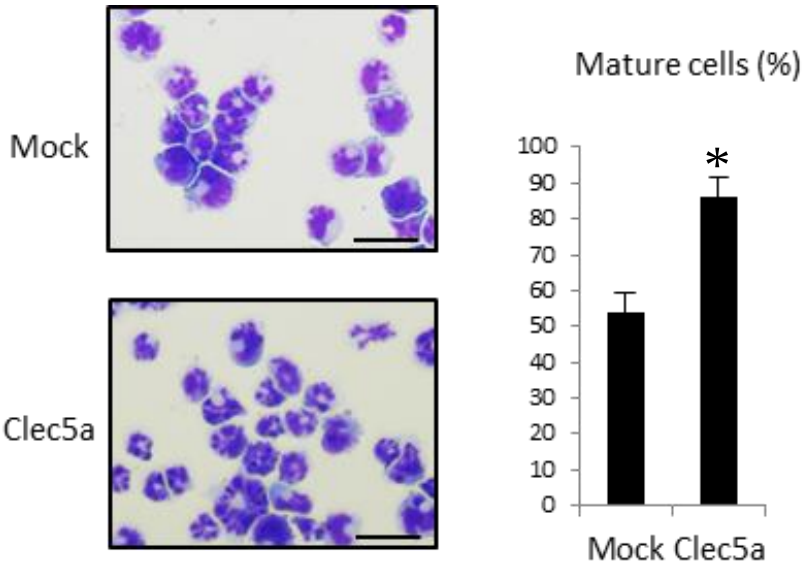

Figure 14. Overexpression of *Clec5a* promoted the differentiation of HL60 cells. (left) Morphology of HL60 cells expressing pMYs-IP (Mock, top) and pMYs-Clec5a-IP (Clec5a, bottom) after incubation with 10^{-6}M ATRA (All-trans Retinoic Acid) for three days. Bars, 20 μm. (right) The proportion of segmented cells. *$P < 0.05$.

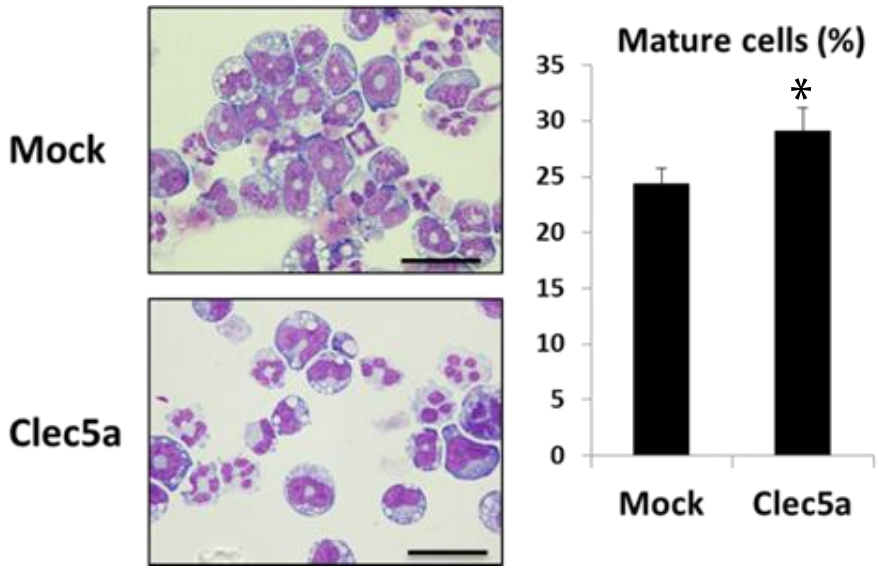

Figure 15. Overexpression of *Clec5a* promoted the differentiation of 32Dcl3 cells. (left) Morphology of 32Dcl3 cells expressing pMYs-IP (Mock, top) and pMYs-Clec5a-IP (Clec5a, bottom) after incubation with 50ng/ml G-CSF for five days. Bars, 20 μm. (right) The proportion of differentiated and segmented cells is shown. *$P < 0.05$.

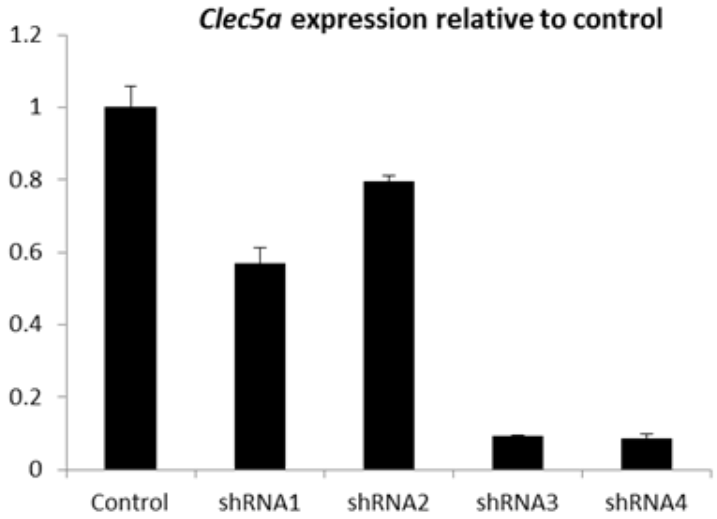

Figure 16. Efficient knocked down of *Clec5a* expression with 2 different anti-*Clec5a* shRNAs compared to control in 32Dcl3 cells as shown by qRT-PCR. These data were normalized by *Gapdh* mRNA. Control indicates pMXs-U6-Puro.

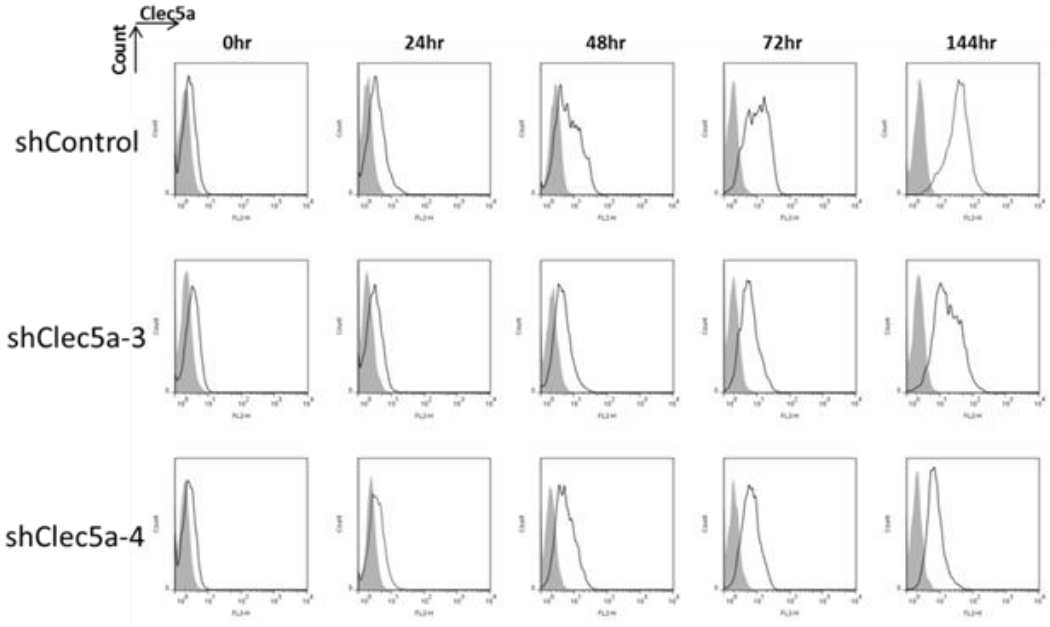

Figure 17. Two shRNAs efficiently inhibited G-CSF induced surface expression of *Clec5a* in Flow cytometric analysis. Filled histograms show control (IgG).

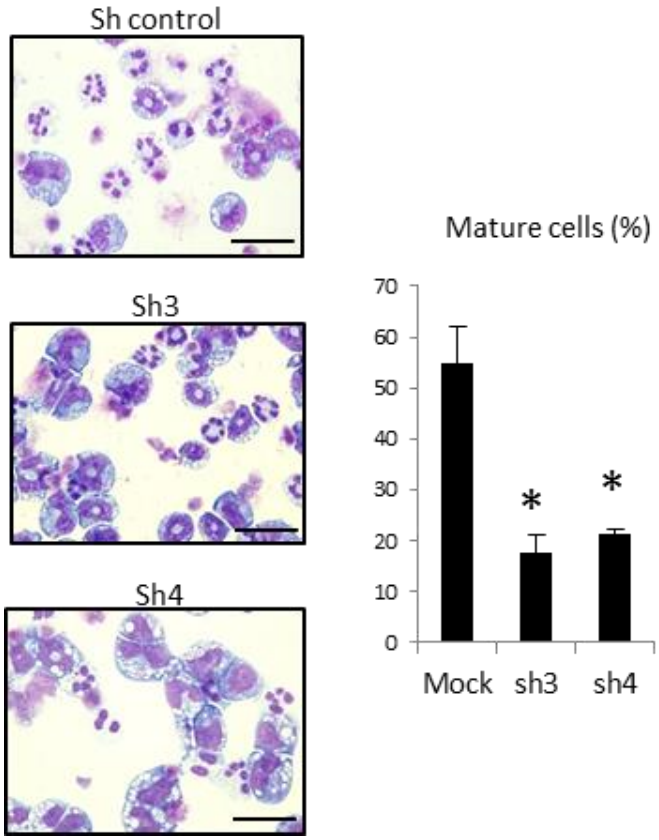

Figure 18. 32Dcl3 cells with or without shRNA for *Clec5a* were incubated with 50ng/ml G-CSF for six days. Morphology (left) and proportion of differentiated 32Dcl3 cells (Right) are shown. Bars, 20 μm. *$P < 0.05$.

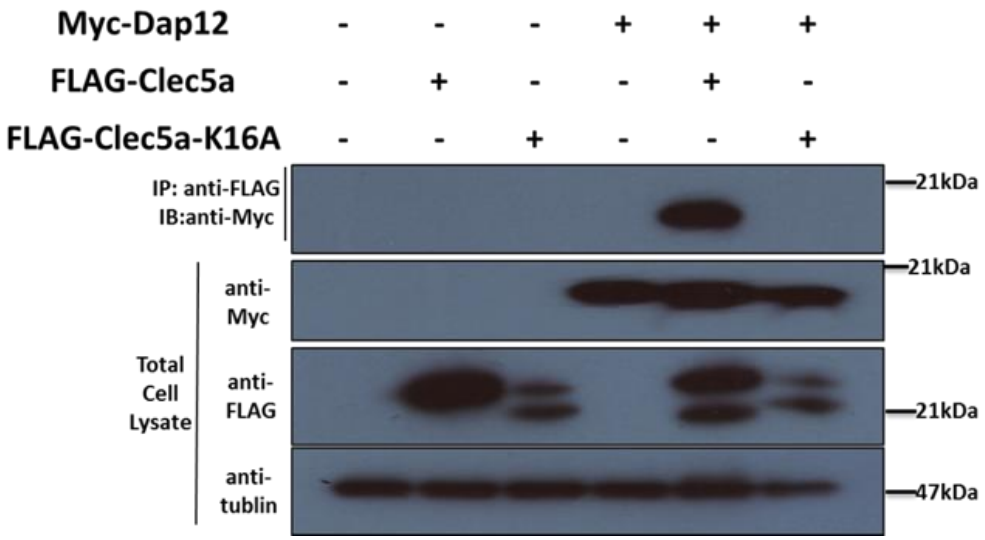

Figure 19. Mutant Clec5a, which harbors a K16A mutation in the transmembrane domain, cannot associate with Dap12, unlike wild-type Clec5a. HEK293T cells were transiently transfected with Myc-Dap12, FLAG-Clec5a, and FLAG-Clec5a-K16A cDNA as described, followed by IP of FLAG epitope and Western blotting for Myc epitope. Total cell lysates were also subject to immunoblotting with anti-Myc Ab or anti-FLAG Ab and anti-tubulin Ab as control.

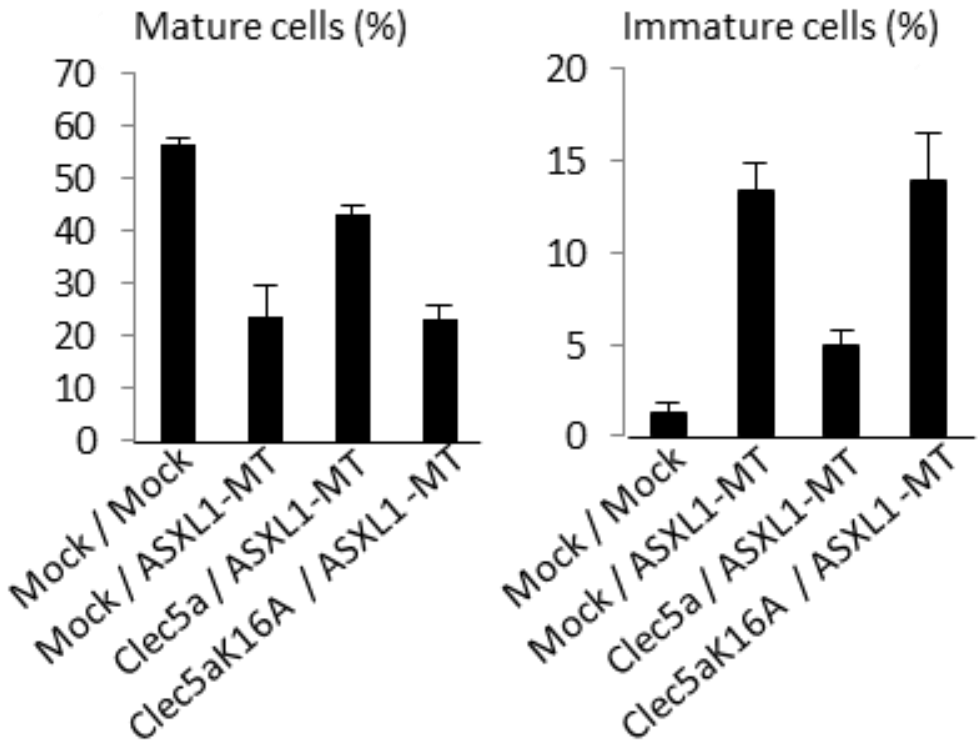

Figure 20. 32Dcl3 cells transduced with pMYs-IP/pMYs-IB, pMYs-IP/ pMYs-ASXL1-MT2-IB, pMYs-Clec5a-IP/pMYs-ASXL1-MT2-IB and pMYs-Clec5a-K16A-IP/pMYs-ASXL1-MT2-IB were cultured in the presence of 50 ng/mL G-CSF for 6 days. The proportion of mature or immature cells are shown.

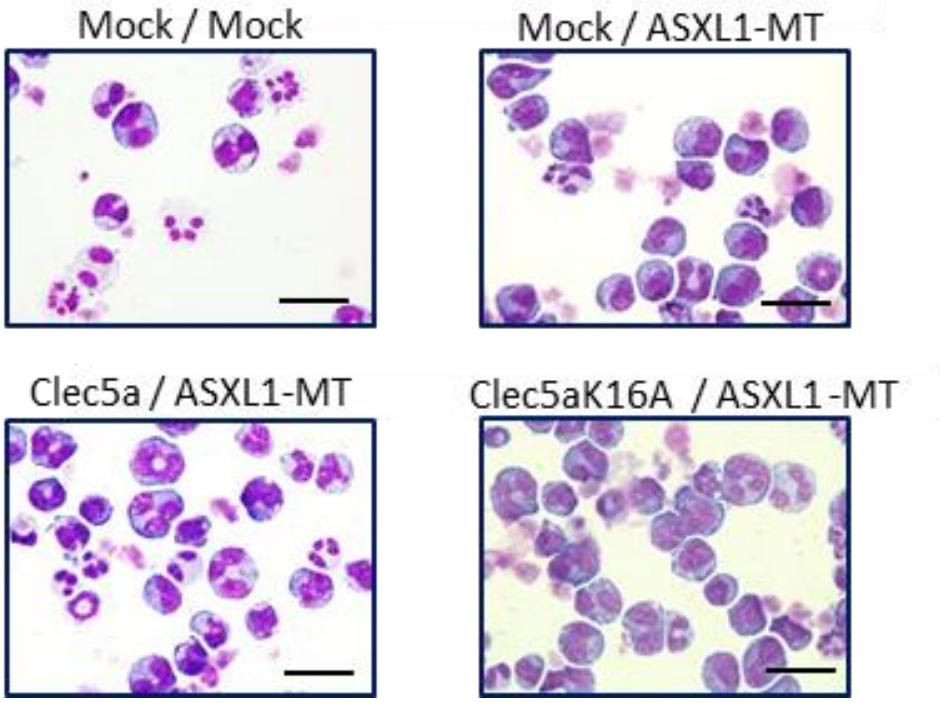

Figure 21. Related to Figure 20, cytospin preparations of these cells are shown. Images were obtained with a BX51 microscope and a DP12 camera (Olympus); objective lens, UplanFl (Olympus); original magnification, ×40; bars, 20 μm. Data are representative of three independent experiments.

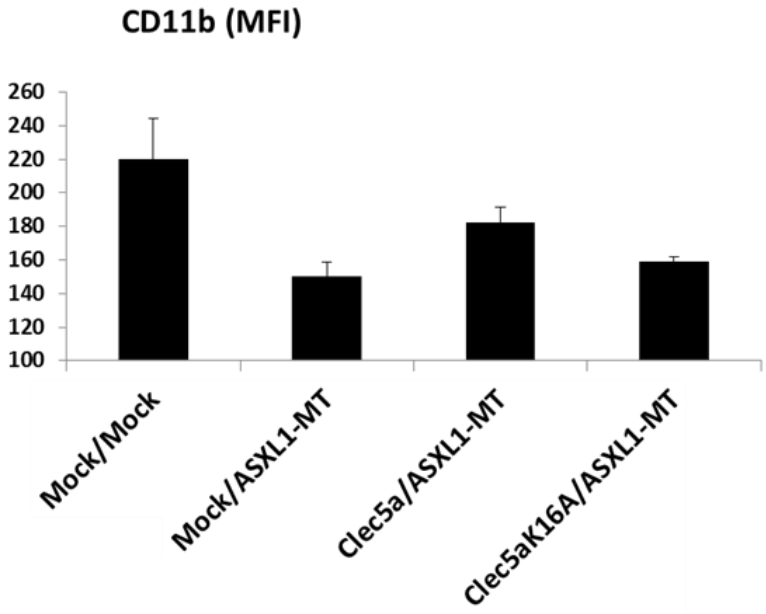

Figure 22. Related to Figure 20, mean fluorescence intensities (MFIs) of CD11b are shown. 32Dcl3 cells transduced with indicated plasmids were incubated with 50 ng/mL G-CSF for 6 days. All data with error bars are presented as mean ± SEM of two independent experiments.

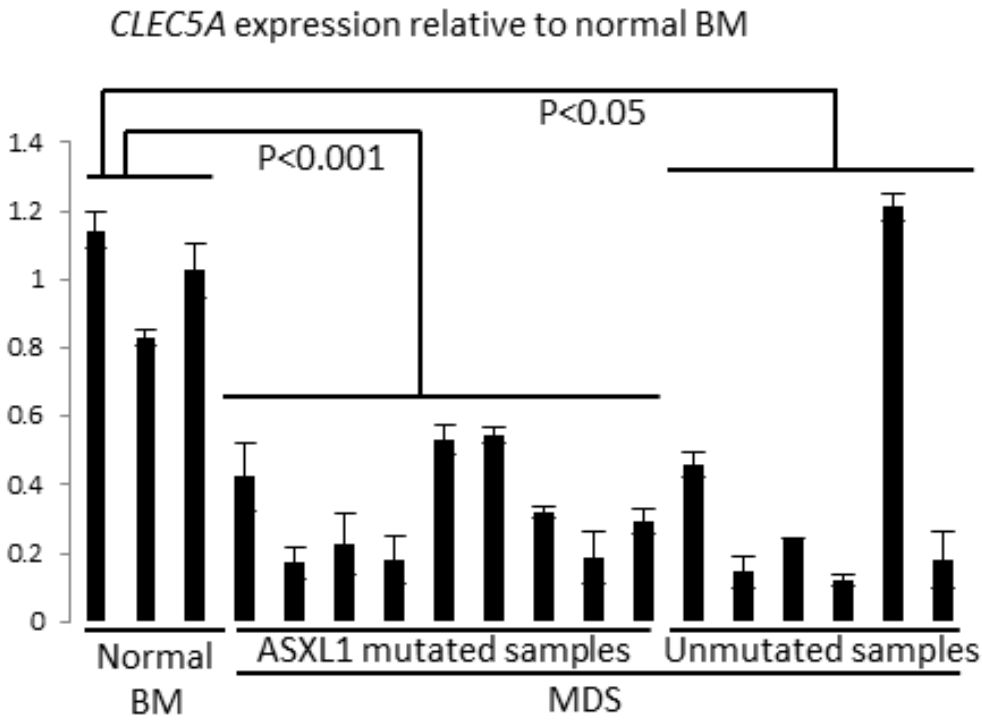

Figure 23. Relative expression levels of *CLEC5A* were examined by qRT- PCR in whole bone marrow cells derived from normal controls and from patients with *ASXL1*-mutated MDS and *ASXL1*-wildtype MDS. The values were normalized by *GAPDH* mRNA levels. All data with error bars are presented as mean ± SEM of two independent experiments. *P*-values were calculated using two tailed Student's t-test or Cochran-Cox test.

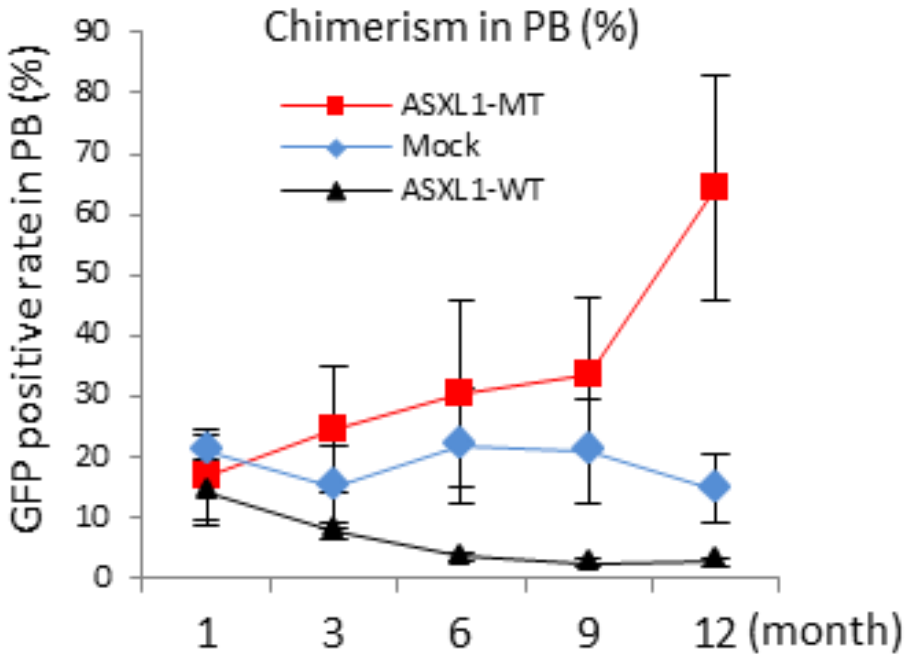

Figure 24. Percent chimerism of donor cells in peripheral blood (PB). The chimerism of Ly-5.1 donor-derived GFP positive cells in PB (mean ± SEM) was examined after transplantation: Mock, n=6; ASXL1-MT, n=12; ASXL1-WT, n=6. *$P < 0.05$.

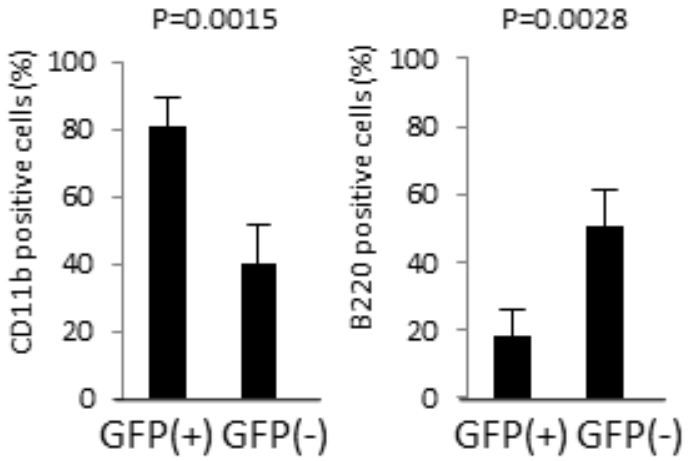

Figure 25. Percentages of CD11b or B220 positive cells related to GFP positivity in the bone marrow (BM) of the transplanted mice determined by flow cytometric analyses. Samples were obtained from mice with pMYs-FLAG-ASXL1-MT2-IG, sacrificed six months after transplantation (n=5). *$P < 0.05$.

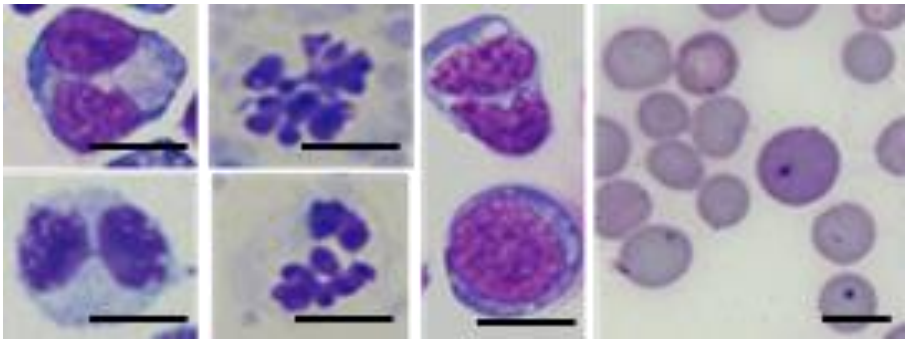

Figure 26. Dysplasias of hematopoietic cells in mice receiving transplants of ASXL1 mutants were observed. Bars, 10 μm.

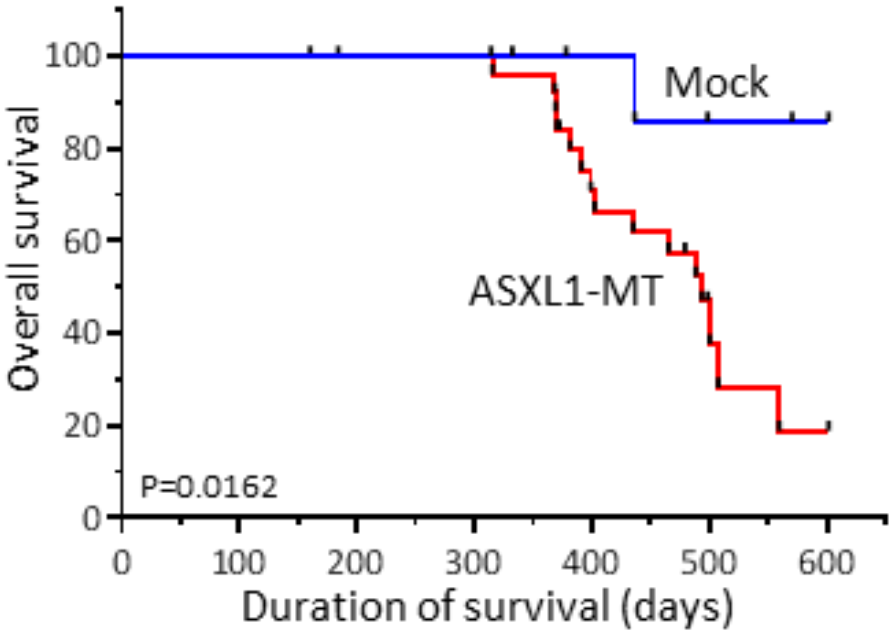

Figure 27. Kaplan-Meier analysis for the survival of mice that received transplants of BM cells transduced with pMYs-IG (Mock, n=13, blue line) and pMYs-FLAG-ASXL1-MT2-IG (ASXL1-MT, n=25, red line). *P*-values were calculated using log-rank test.

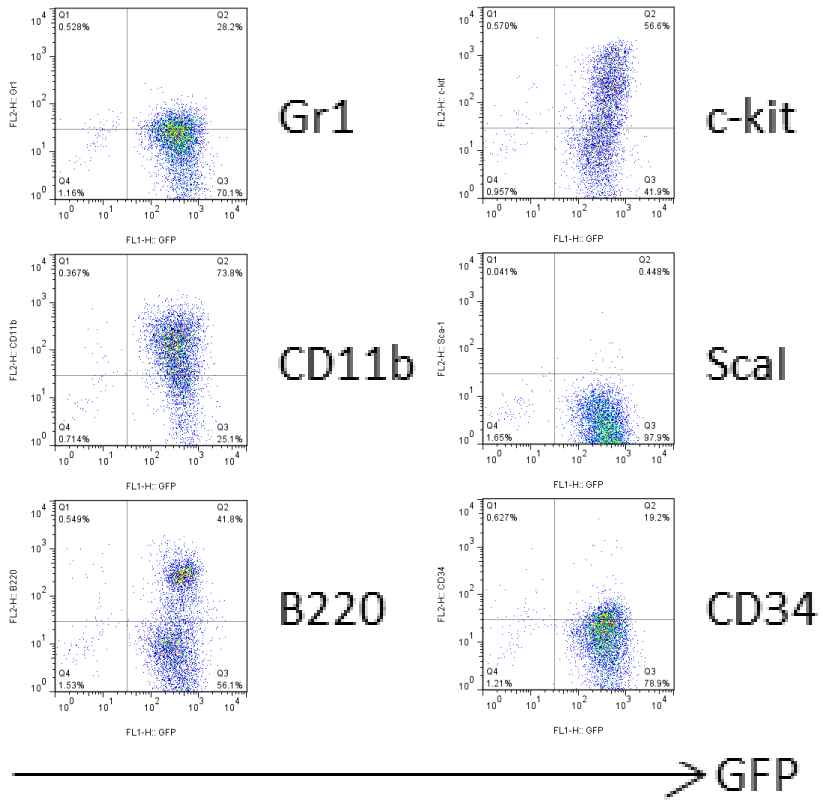

Figure 28. Flow cytometric analyses of BM cells derived from mice with ASXL1-MT.

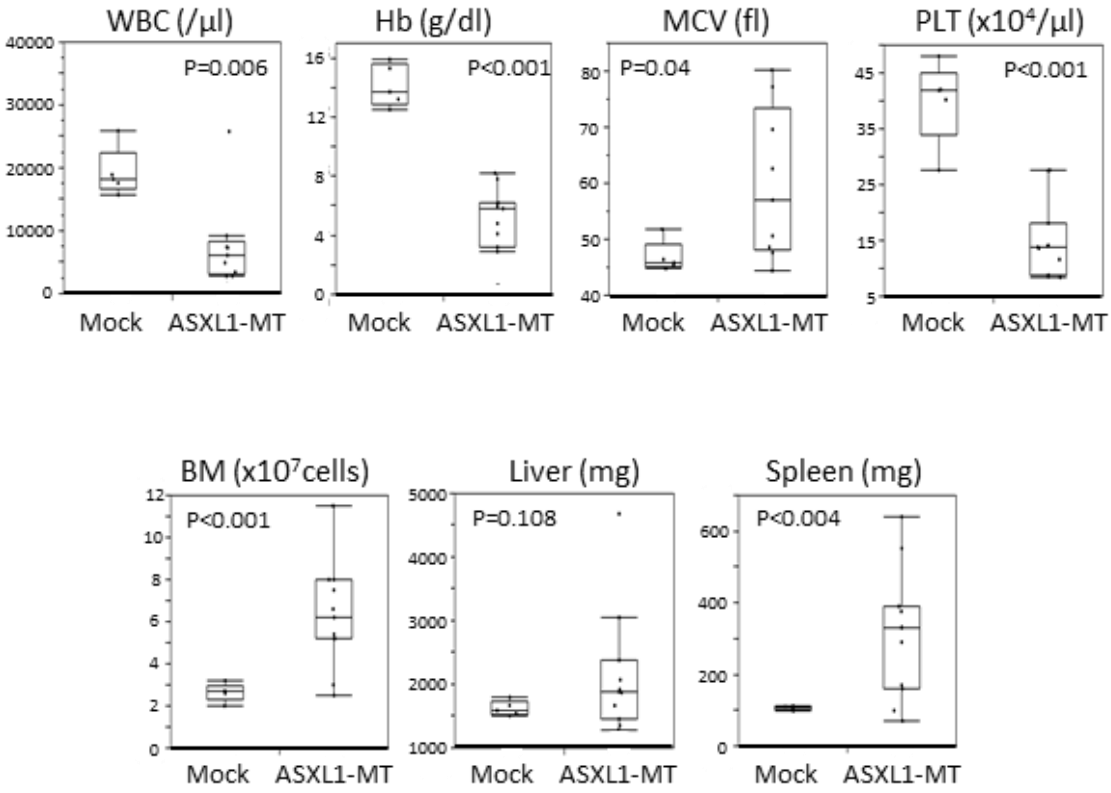

Figure 29. Mice transplanted with ASXL1-MT2 (ASXL1-MT, n=11) displayed progressive pancytopenia, macrocytosis, hyperplastic BM, and increased splenomegaly compared with mice transplanted with empty vector (Mock, n=5). BM cells were isolated from the femurs and tibias of the sacrificed mice.

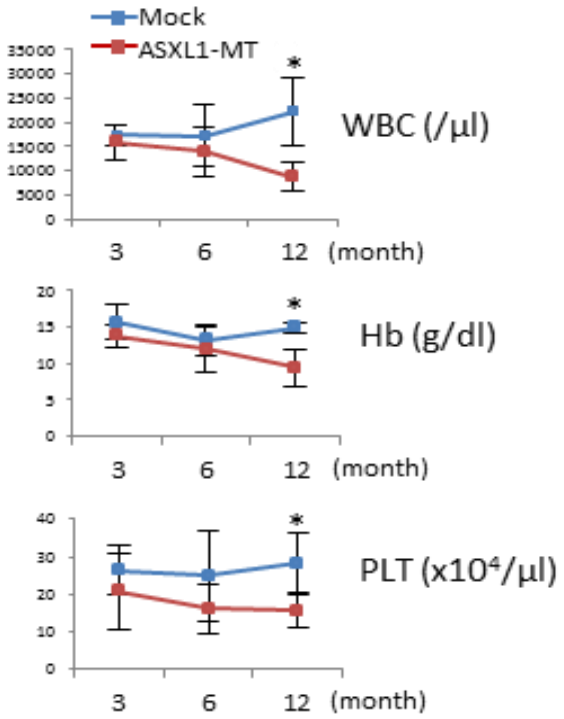

Figure 30. Blood count data, including WBC, Hb, and PLT, at 3, 6, or 12 months after transplantation are indicated (mean ± SEM): Mock, n=6; ASXL1-MT, n=12. *$P < 0.05$.

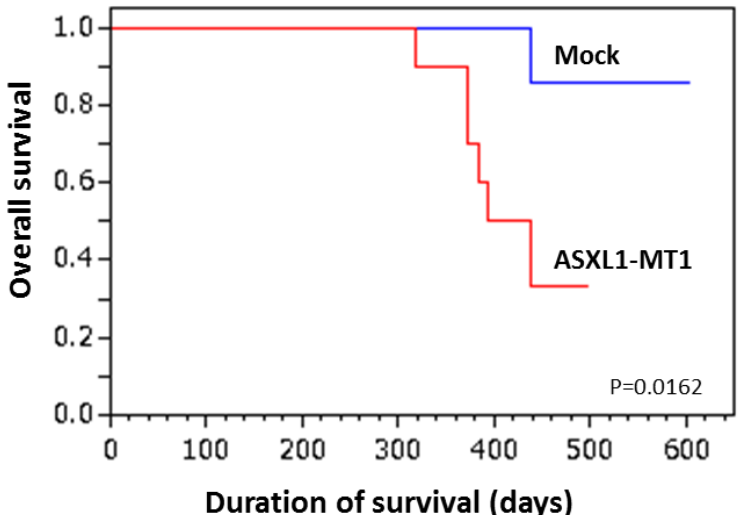

Figure 31. Kaplan-Meier analysis for the survival of mice that received transplants of BM cells transduced with pMYs-IG (Mock, n=13, blue line) and pMYs-FLAG-ASXL1-MT1-IG (ASXL1-MT1, n=10, red line). *P*-values were calculated using log-rank test.

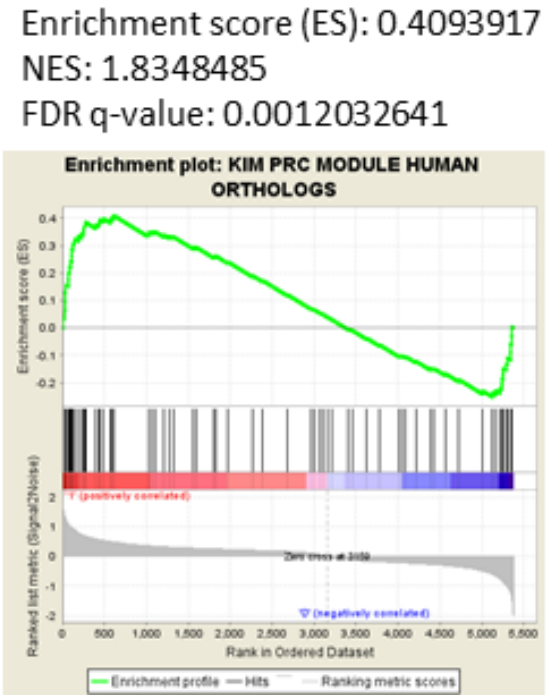

Figure 32. GSEA of microarray analysis of mice with ASXL1-MT revealed a significant enrichment of genes found in a previously described gene expression signature of the PRC target, compared to that of mice with empty vectors.

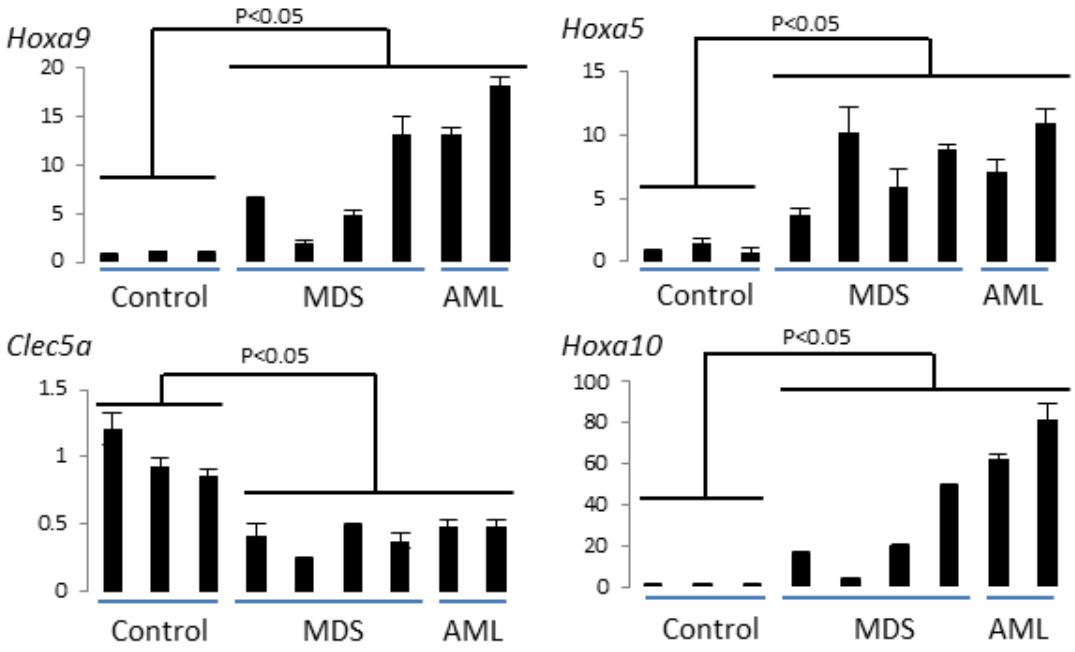

Figure 33. In the mouse BMT model, ASXL1-MT-induced MDS/AML resulted in increased *Hoxa5*, *Hoxa9*, and *Hoxa10* and decreased *Clec5a* mRNA expression as shown by qRT-PCR analysis in BM cells from transplanted mice.

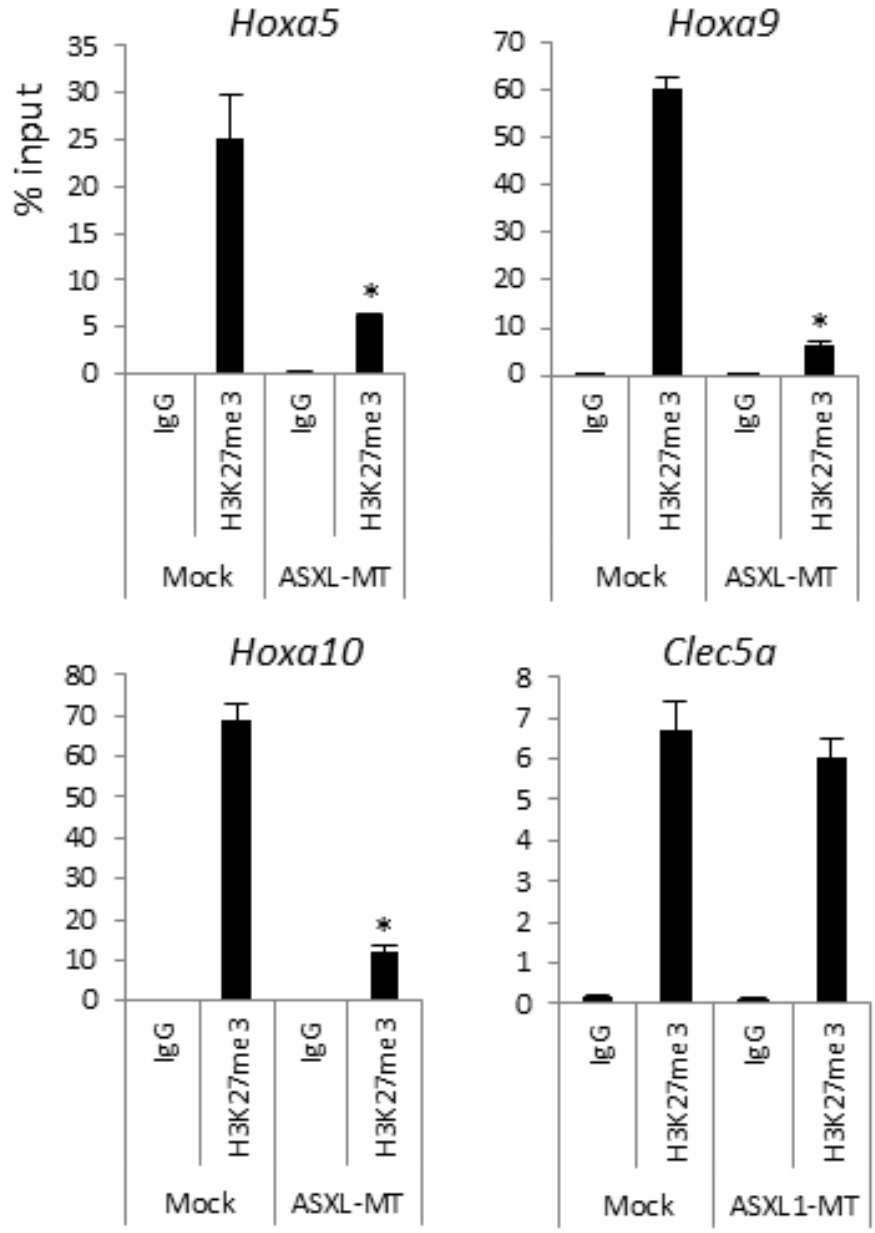

Figure 34. ChIP for H3K27me3 followed by qPCR across the *Hoxa5*, *Hoxa9*, *Hoxa10*, and *Clec5a* locus in BM cells of mice that received transplants of BM cells transduced with pMYs-IG (Mock) or pMYs-FLAG-ASXL1-MT-IG (ASXL1-MT).

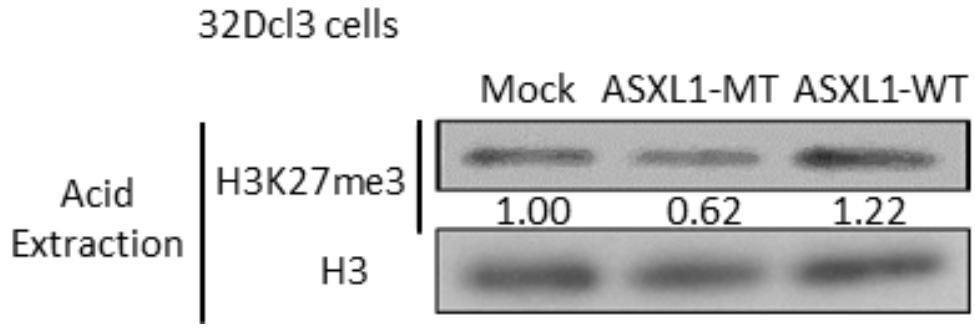

Figure 35. Acid-extracted histones were obtained from 32Dcl3 cells transduced with pMYs-IG, pMYs-FLAG–ASXL1-MT-IG, and pMYs-FLAG-ASXL1-WT-IG, and then analyzed by Western blotting using anti-H3K27me3 antibodies. Levels of histone modifications were normalized to the amount of histone H3 and are indicated using ImageJ (http://rsbweb.nih.gov/ij/download.html).

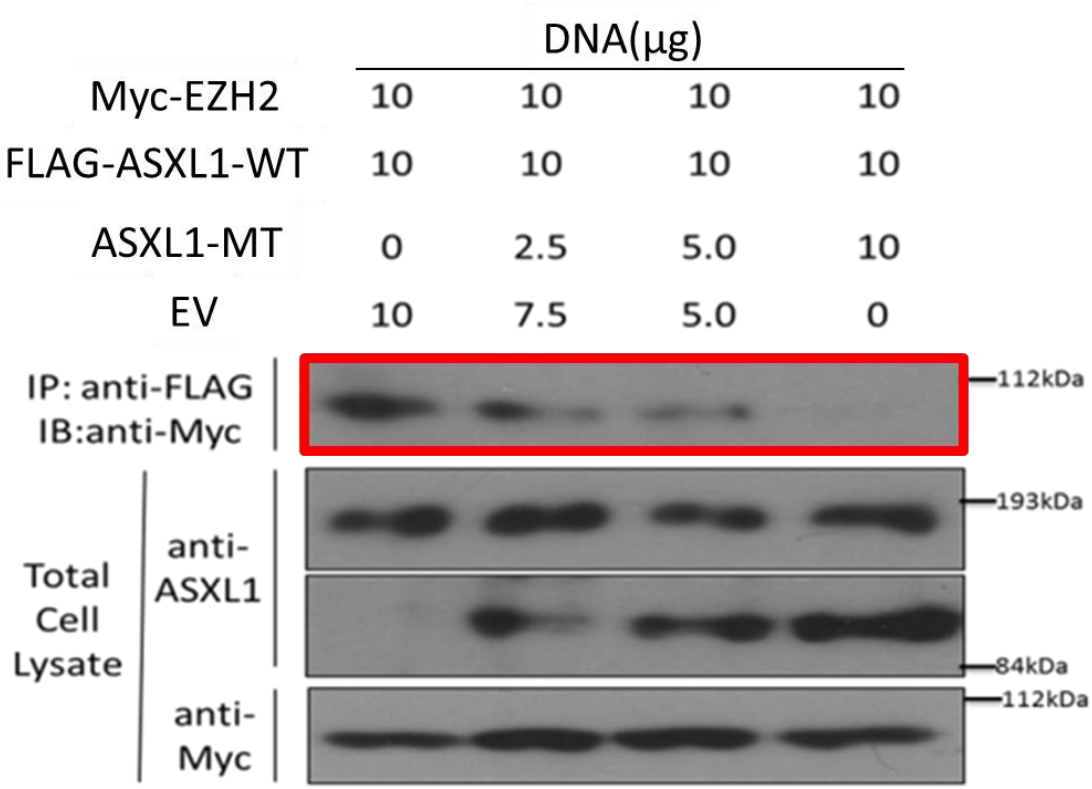

Figure 36. ASXL1-MT efficiently inhibited the interaction between ASXL1-WT and EZH2 (red square). HEK293T cells were transiently transfected with indicated amounts (μg) of Myc-EZH2, FLAG-ASXL1-WT, and ASXL1-MT expressing vectors followed by IP of FLAG epitope and Western blotting for Myc epitope. Cell lysates were also subjected to immunoblotting with anti-FLAG Ab or anti-Myc Ab. The results shown are representative of three independent experiments.

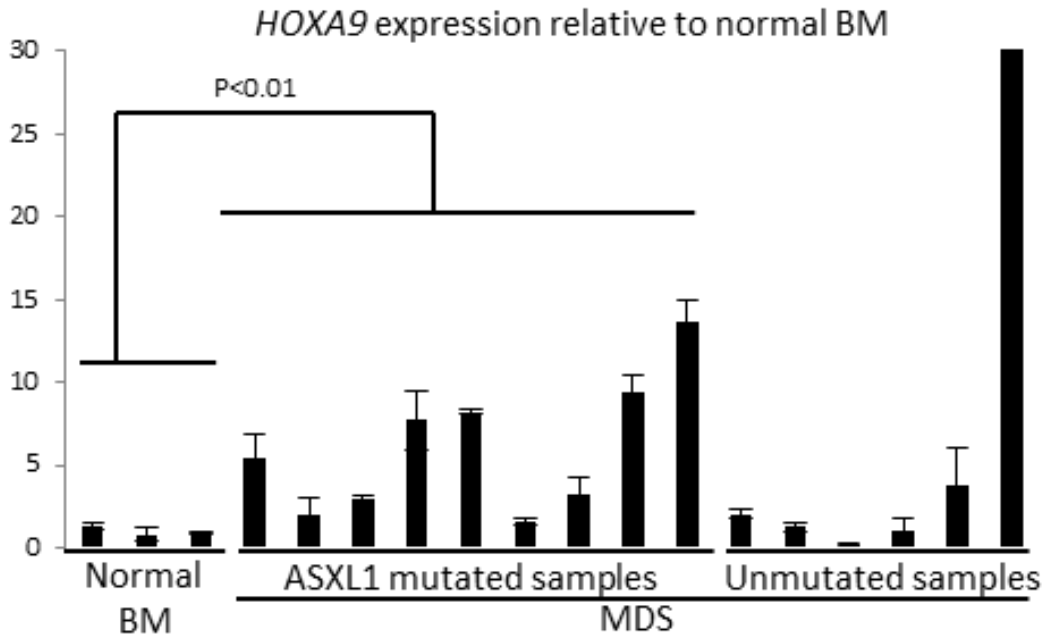

Figure 37. Relative expression levels of *HOXA9* were examined by qRT-PCR in whole BM cells derived from normal controls and from patients with *ASXL1*-mutant MDS and *ASXL1*-wildtype MDS. The values were normalized by GAPDH mRNA levels.

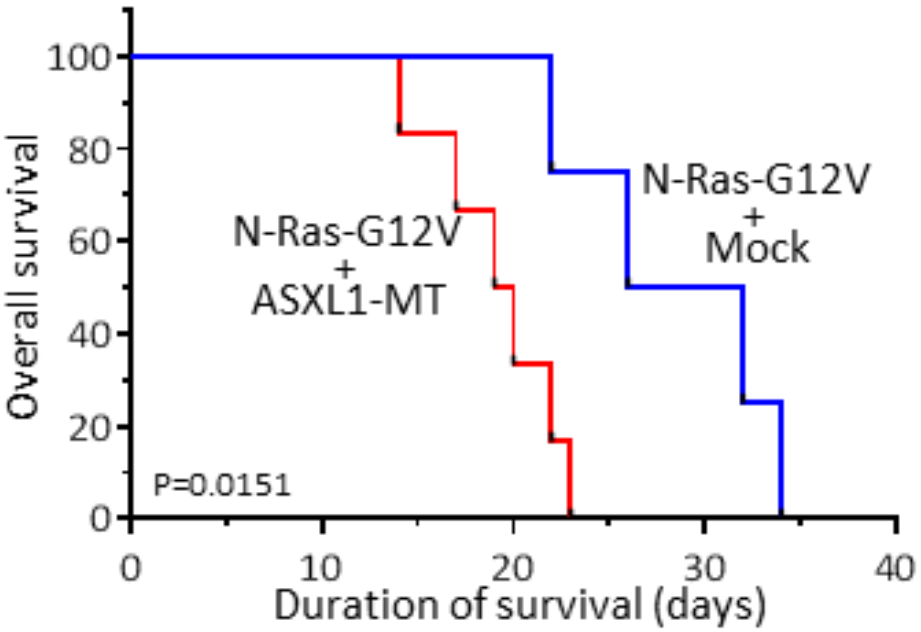

Figure 38. Kaplan-Meier analysis for the survival of mice that received transplants of BM cells transduced with pMYs-N-Ras-G12V-IG and pMYs-INGFR (N-Ras-G12V + Mock, n=4, blue line) and pMYs-N-Ras-G12V-IG and pMYs-ASXL1-MT2-INGFR (N-Ras-G12V + ASXL1-MT, n=6, red line). *P*-values were calculated using log-rank test.

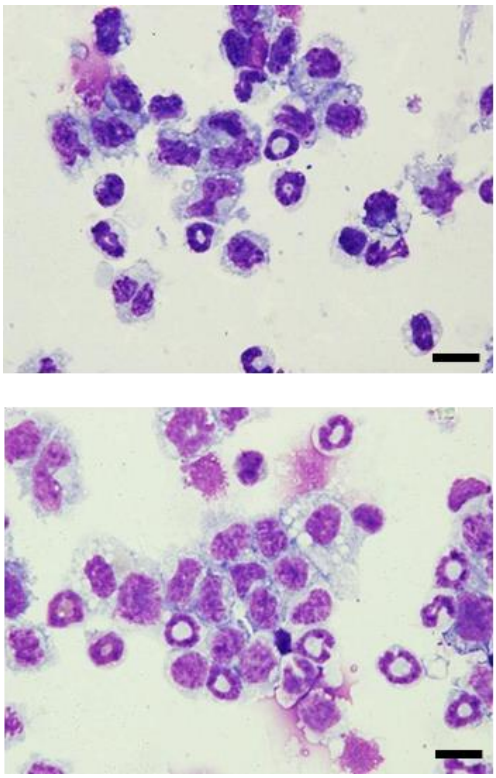

Figure 39. Cytospin preparations of BM cells derived from mice transplanted with N-Ras-G12V + Mock and N-Ras-G12V + ASXL1-MT were stained with Giemsa. Representative photographs are shown. Original magnification, x400; bars, 20 μm.

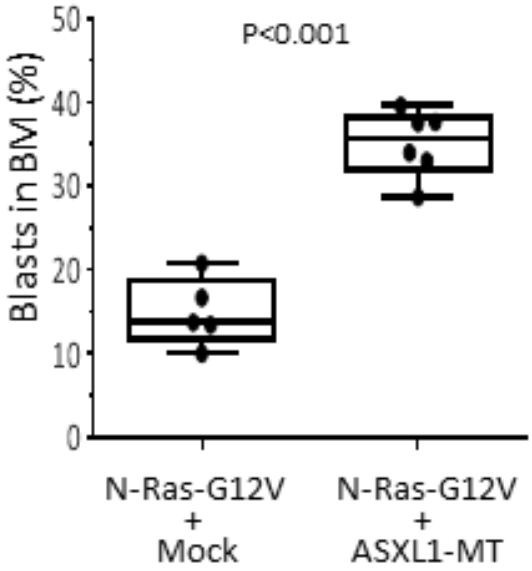

Figure 40. Mice transplanted with N-Ras-G12V/ASXL1-MT displayed increased numbers of leukemic blasts in BM. *P*-values were calculated using the Student's t-test.

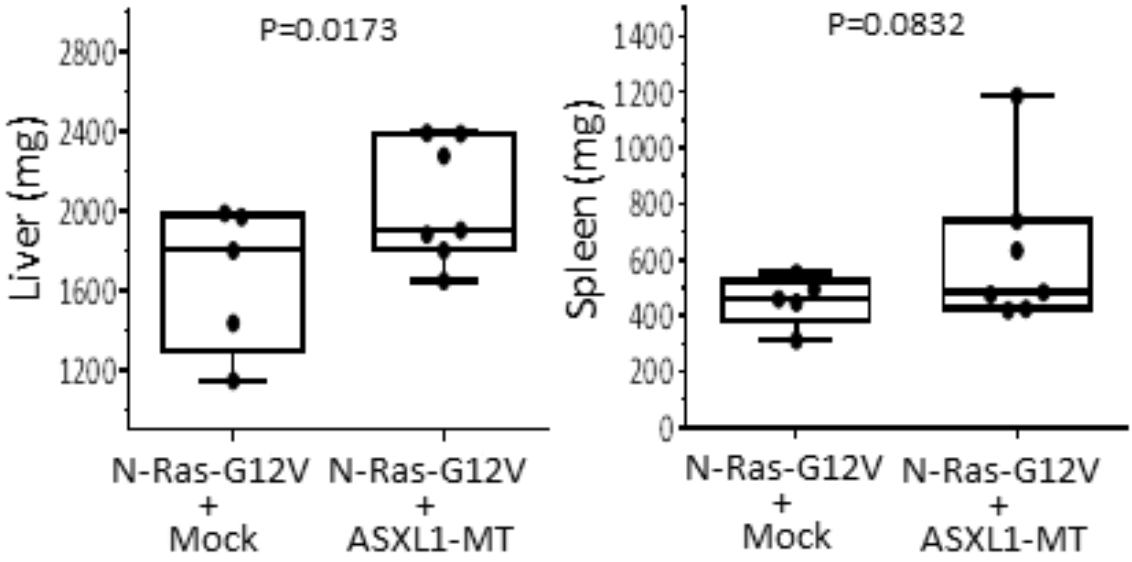

Figure 41. Mice transplanted with N-Ras-G12V/ASXL1-MT displayed hepatomegaly and splenomegaly, although the differences in spleen weight were not statistically significant. *P*-values were calculated using Cochran-Cox test.

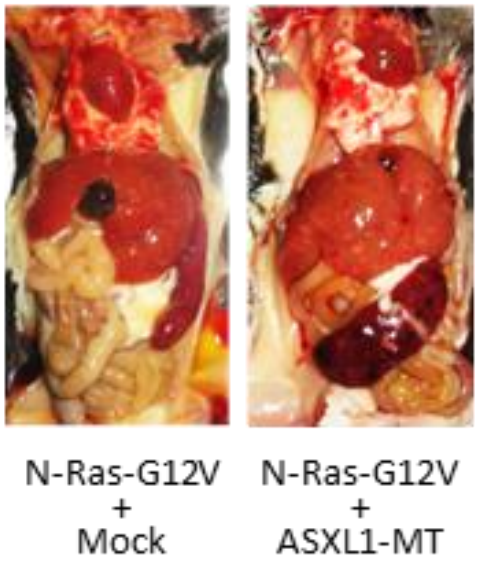

Figure 42. Macroscopic findings of sacrificed mice transplanted with BM cells transduced with indicated construct. Representative photographs are shown.

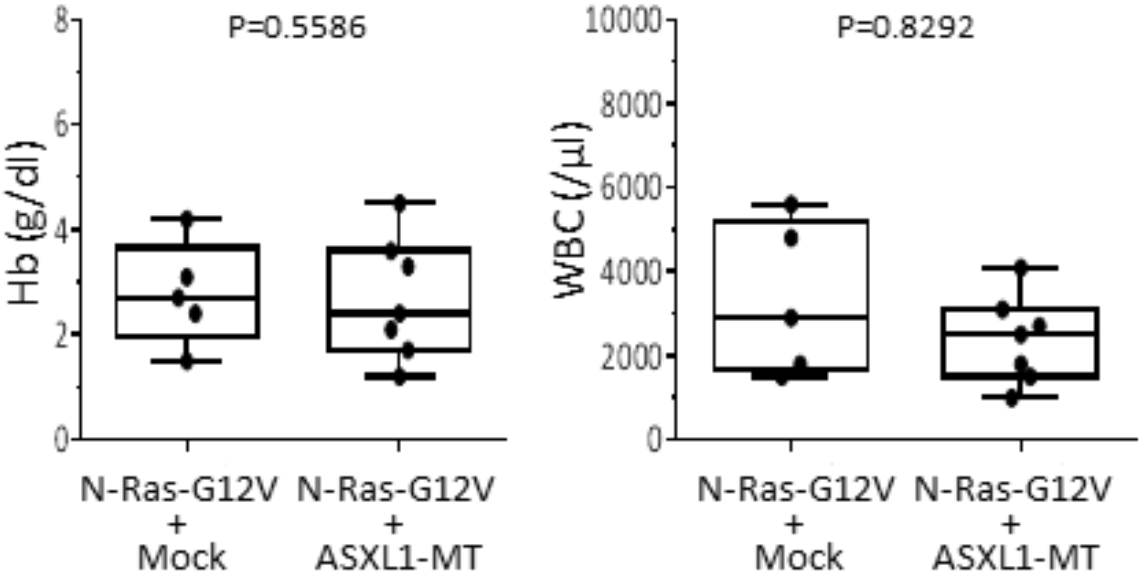

Figure 43. Mice transplanted with N-Ras-G12V/Mock and N-Ras-G12V/ASXL1-MT displayed severe anemia and leukopenia to a similar extent.

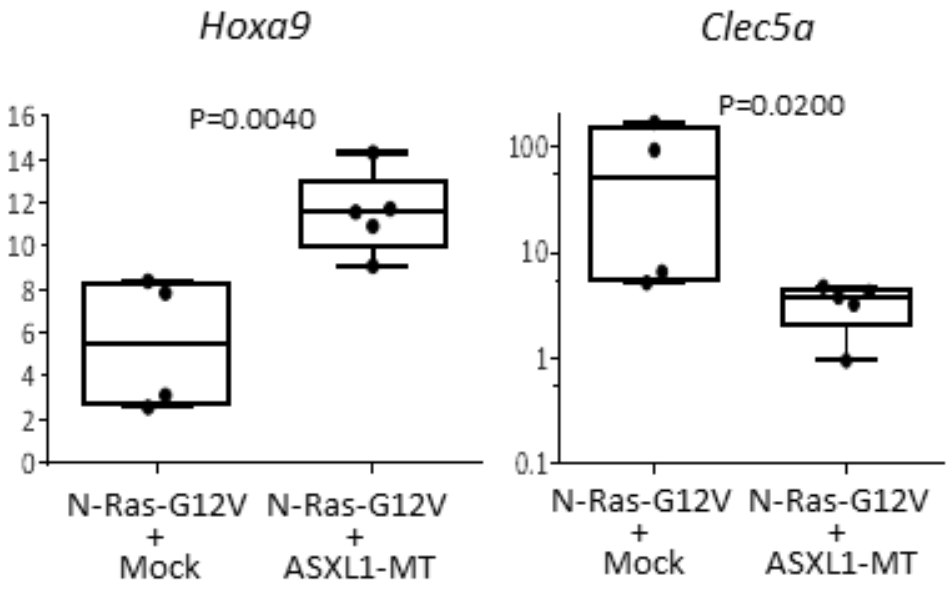

Figure 44. qRT-PCR revealed an increased expression of *Hoxa9* and decreased expression of *Clec5a* in the BM of mice transplanted with N-Ras-G12V/ASXL1-MT. *P*-values were calculated using the Cochran-Cox test.

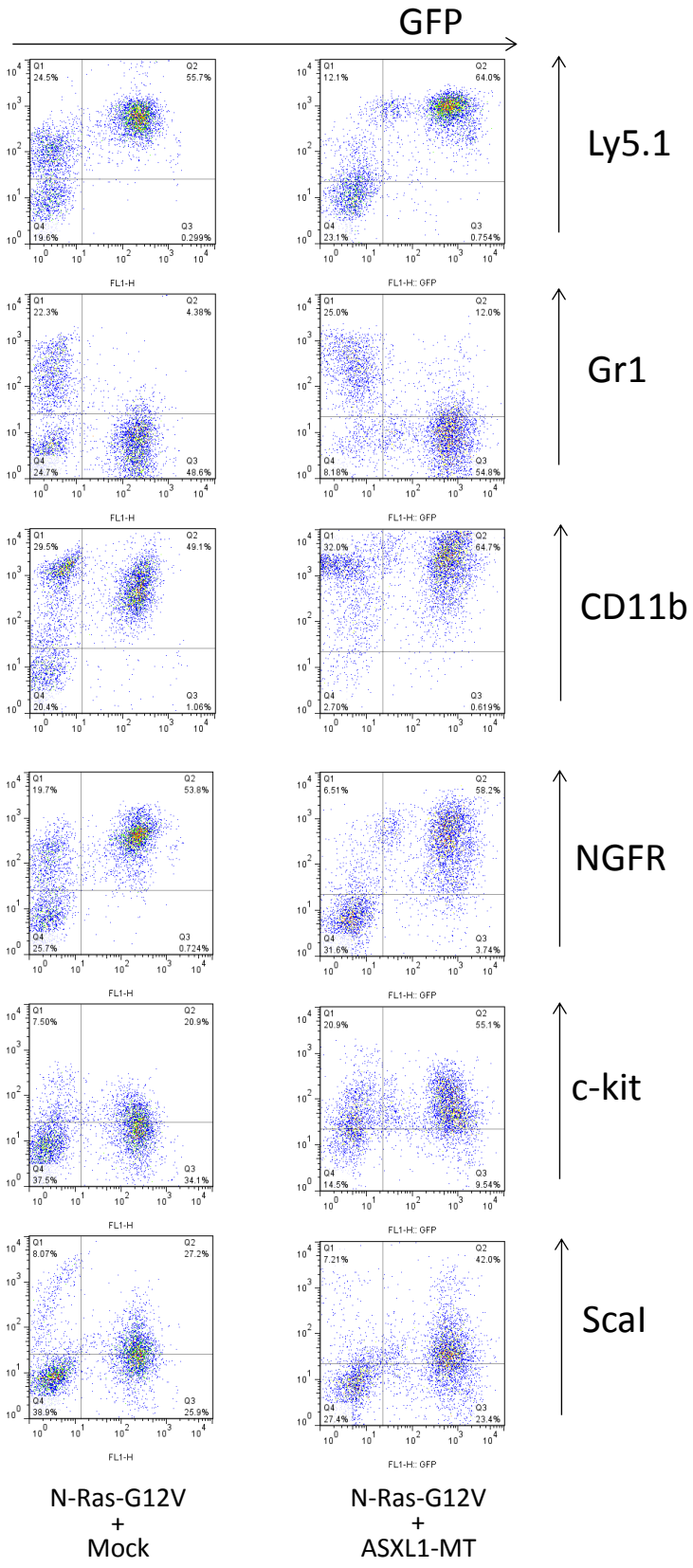

Figure 45. Flow cytometric analysis of BM cells derived from sacrificed mice transduced with indicated constructs.

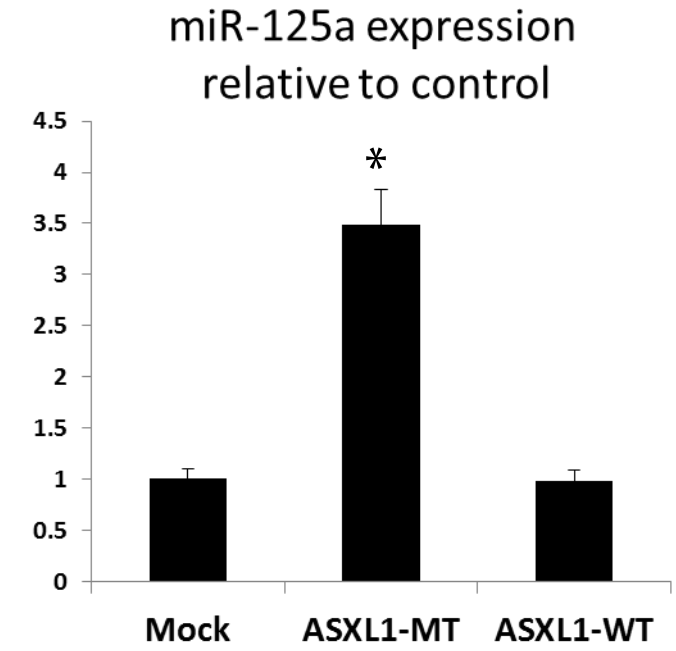

Figure 46. Overexpression of ASXL1-MT, not ASXL1-WT, induced the expression of miR-125a. qRT-PCR for miR-125a in 32Dcl3 cells transduced with pMYs-IG, pMYs-FLAG-ASXL1-MT2-IG, pMYs-FLAG-ASXL1-WT. Relative expression levels normalized by RNU6B (RNA, U6 small nuclear 2) were shown. *$P < 0.05$.

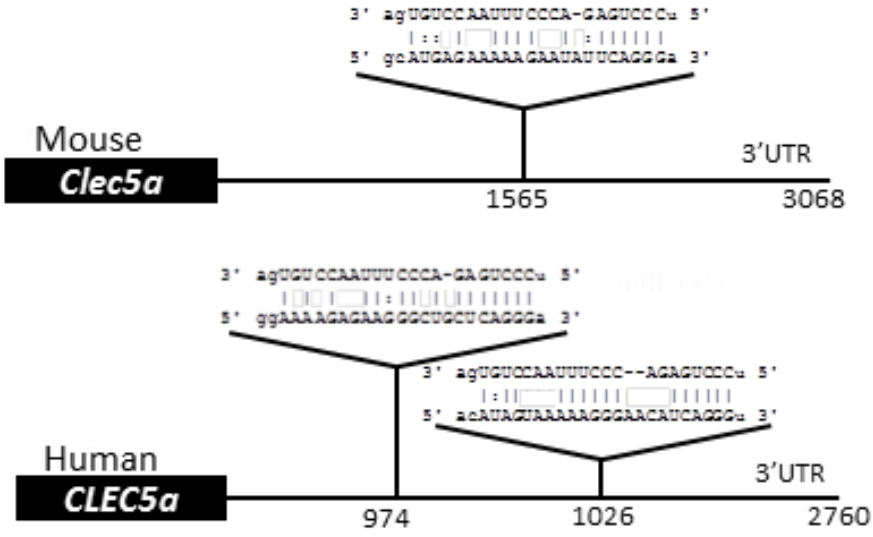

Figure 47. Schematic presentation of predicted miR-125a–binding sites in the mouse *Clec5a* (top) and human *CLEC5A* 3′UTR (bottom).

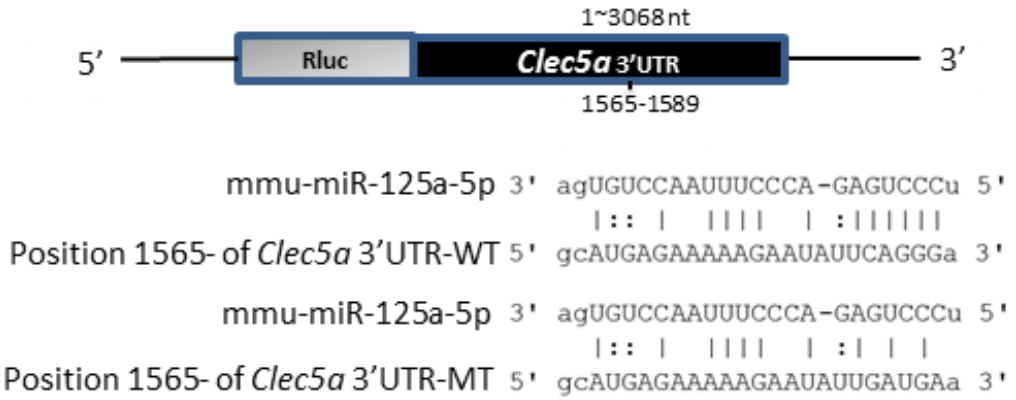

Figure 48. To confirm that *Clec5a* is a direct target gene of miR-125a, the wild-type 3'UTR of *Clec5a* or the mutated 3'UTR was cloned to downstream of the Renilla luciferase (Rluc) open reading frame. Schematic diagrams of predicted miR-125a–binding sites in the *Clec5a*-3'UTR and the alignment between miR-125a and either *Clec5a*-3'UTR (top) or a mutated 3'UTR (bottom) are shown. Three bases in the 3'UTR, corresponding to seed sequences, were replaced with the indicated bases in the mutant form.

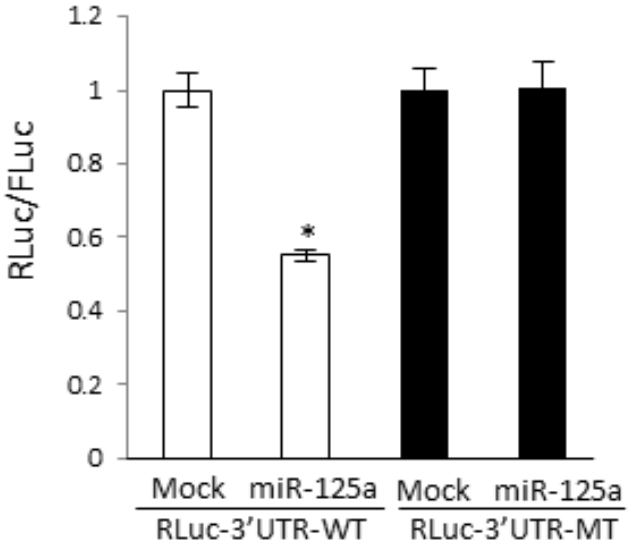

Figure 49. 293T cells were cotransfected with an internal control vector (pGL3-control), and either pGL4.74[hRluc/TK]-Clec5a3'UTR-WT or pGL4.74[hRluc/TK]-Clec5a3'UTR-MT and either pMXs-EF1-miR-125a-Puro or mock (pMXs-EF1-Puro). Luciferase assays were performed with a triplicate set. **P* < 0.05.

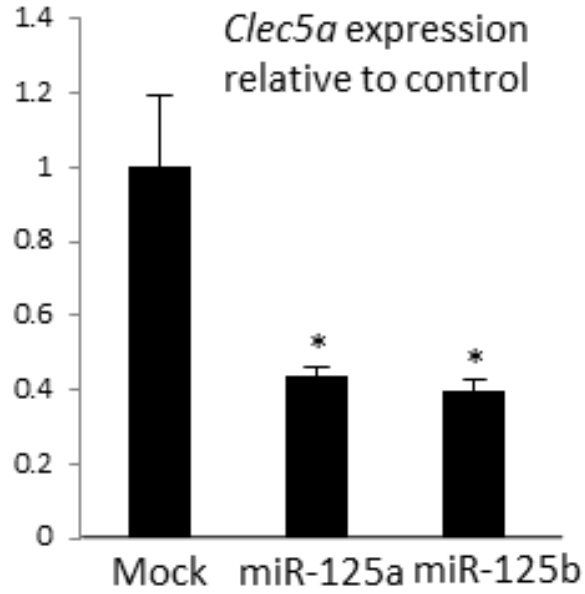

Figure 50. Relative expression levels of *Clec5a* by qRT-PCR in 32Dcl3 cells transduced with pMXs-EF1-Puro (Mock), pMXs-EF1-miR-125a-Puro, and pMXs-EF1-miR-125b-Puro. **P* < 0.05.

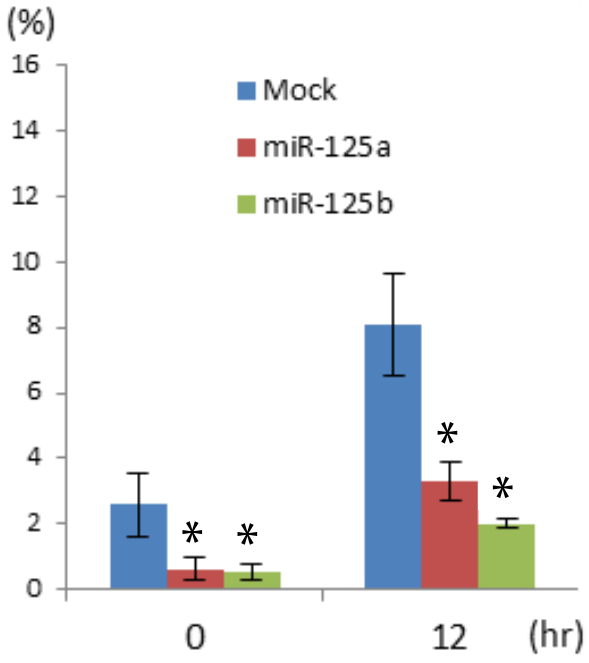

Figure 51. Positive rate of Clec5a expression in 32Dcl3 cells transduced with mock, miR-125a or miR-125b after incubation with 1ng IL-3 (0hr) or 50 ng/ml G-CSF (12hr) was analyzed by flow cytometry at indicated time points. **P* < 0.05.

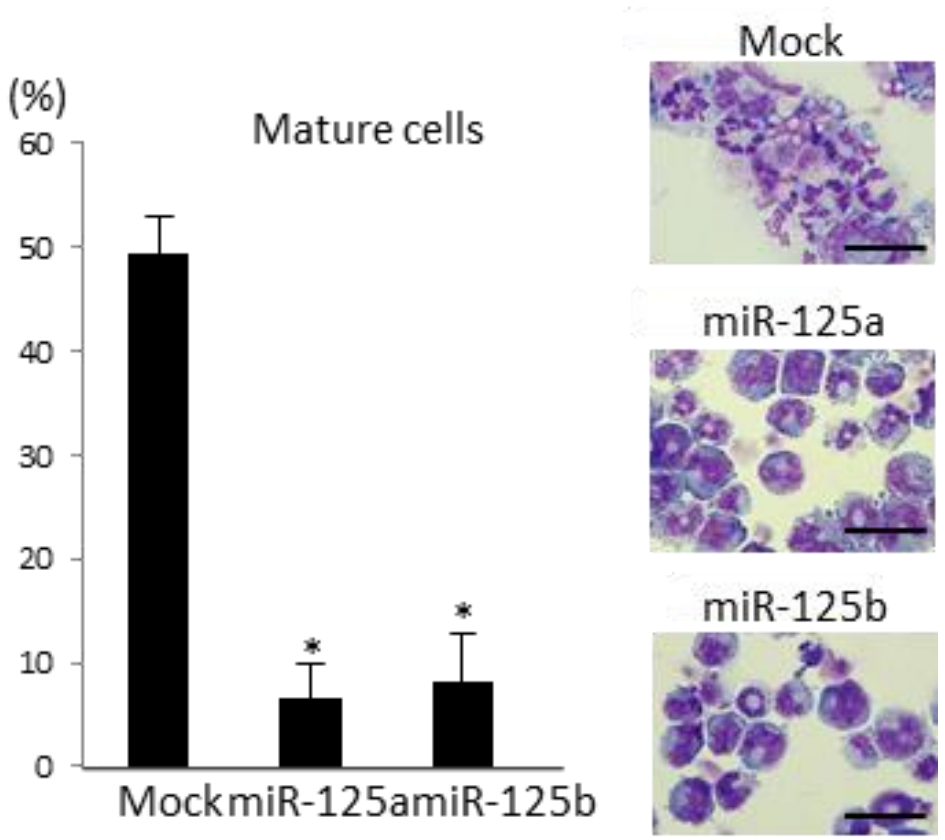

Figure 52. The proportion of mature cells (left) and cytospin preparations (right) of the 32Dcl3 cells expressing mock, miR-125a or miR-125b cultured in the presence of 50 ng/mL G-CSF for six days. Bars, 20 μm. *$P < 0.05$.

Figure 53. Schematic diagram of the mmu-miR-125a and Ncrna00085 loci indicating their genomic structures. Exons are demarcated by black boxes. Regions amplified from the precipitated DNA by site-specific quantitative PCR are indicated by arrows.

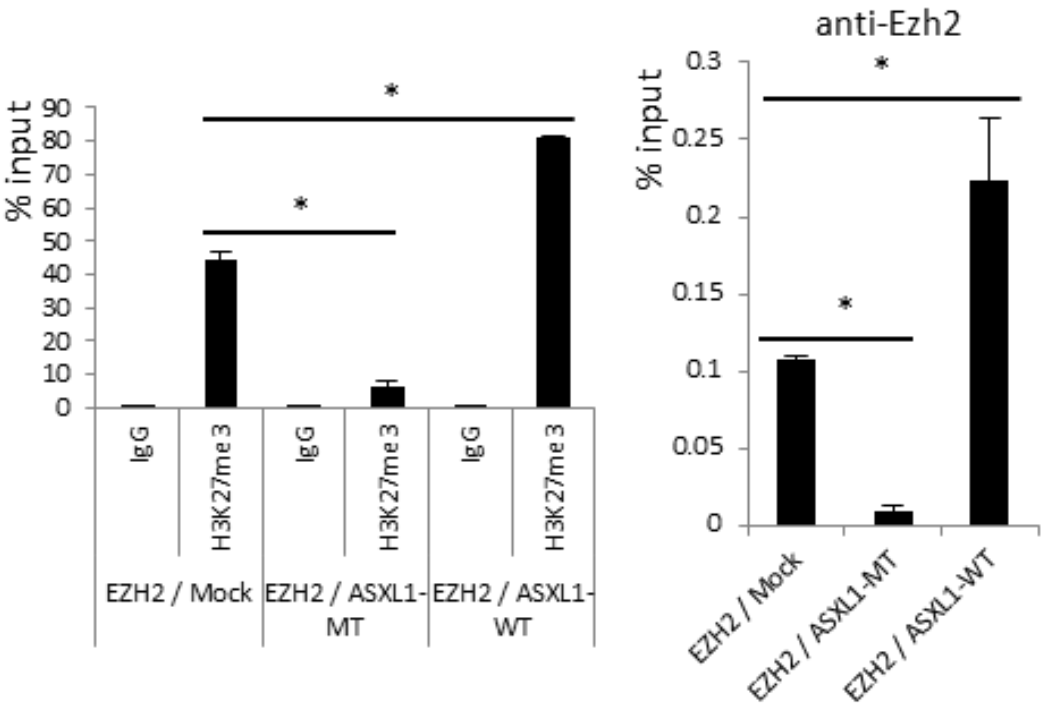

Figure 54. Quantitative ChIP analyses of 32Dcl3 cells transduced with pMYs-EZH2-IG and pMYs-IP (EZH2/Mock), pMYs-EZH2-IG and pMYs-FLAG-ASXL1-MT2-IP (EZH2/ASXL1-MT), or pMYs-EZH2-IG and pMYs-FLAG-ASXL1-WT-IP (EZH2/ASXL1-WT). Abs specific to H3K27me3 or Ezh2 and primers for miR-125a-2 were used. There were no detectable or very low levels of background signals with IgG isotype controls at all amplified regions. Percentages of input DNA are shown as the mean ± SEM for duplicate analyses. *$P < 0.05$. Data are representative of three independent experiments.

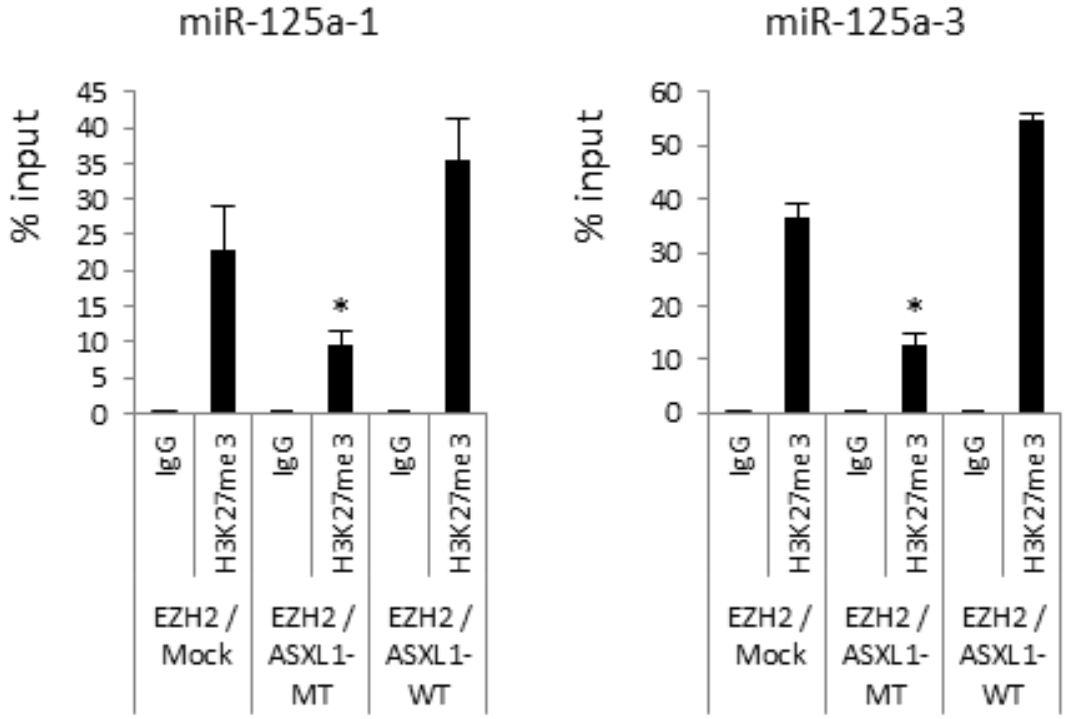

Figure 55. Related to Figure 54, ChIP analyses of 32Dcl3 cells were performed using primers for miR-125a-1/3.

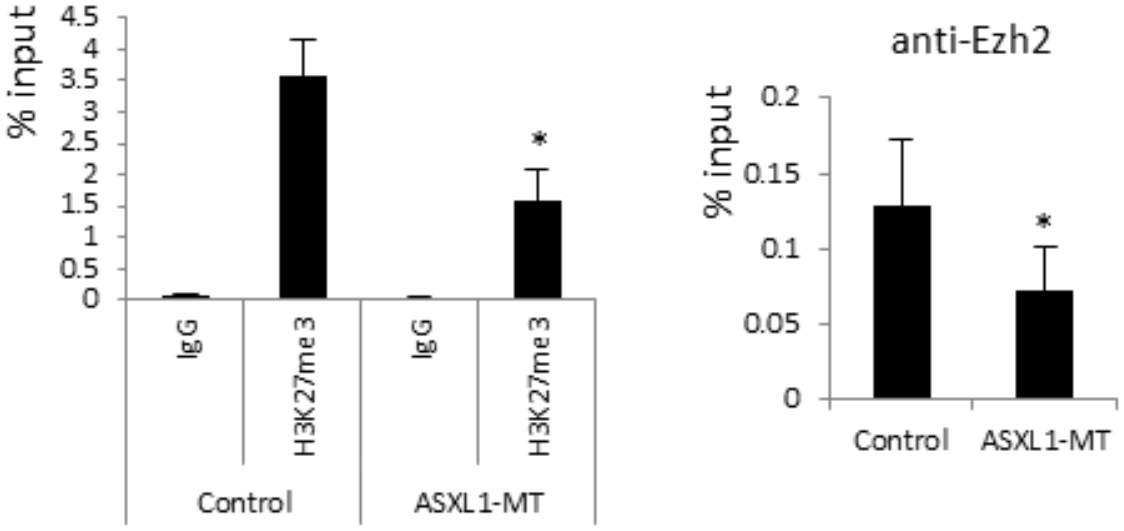

Figure 56. Quantitative ChIP analyses of BM cells from the mice transplanted with BM cells transduced with pMYs-IG (Mock) or pMYs-FLAG-ASXL1-MT2 (ASXL1-MT). Abs specific to H3K27me3 or Ezh2 and primers for miR-125a-2 were used for ChIP analyses. There were no detectable or very low levels of background signals with IgG isotype controls at all amplified regions. Percentages of input DNA are shown as the mean ± SEM for duplicate analyses. **P* < 0.05. Data are representative of three independent experiments.

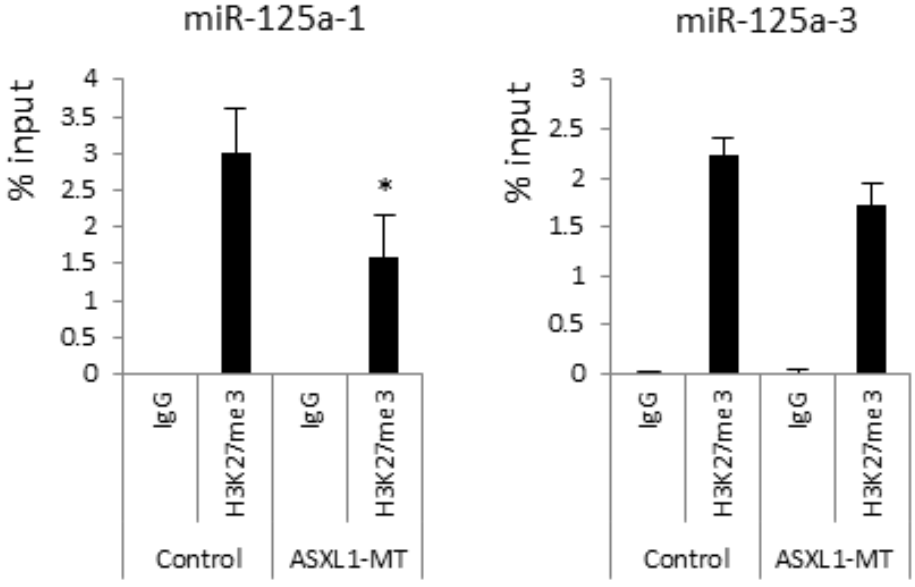

Figure 57. Related to Figure 56, ChIP analyses of BM cells were performed using primers for miR-125a-1/3.

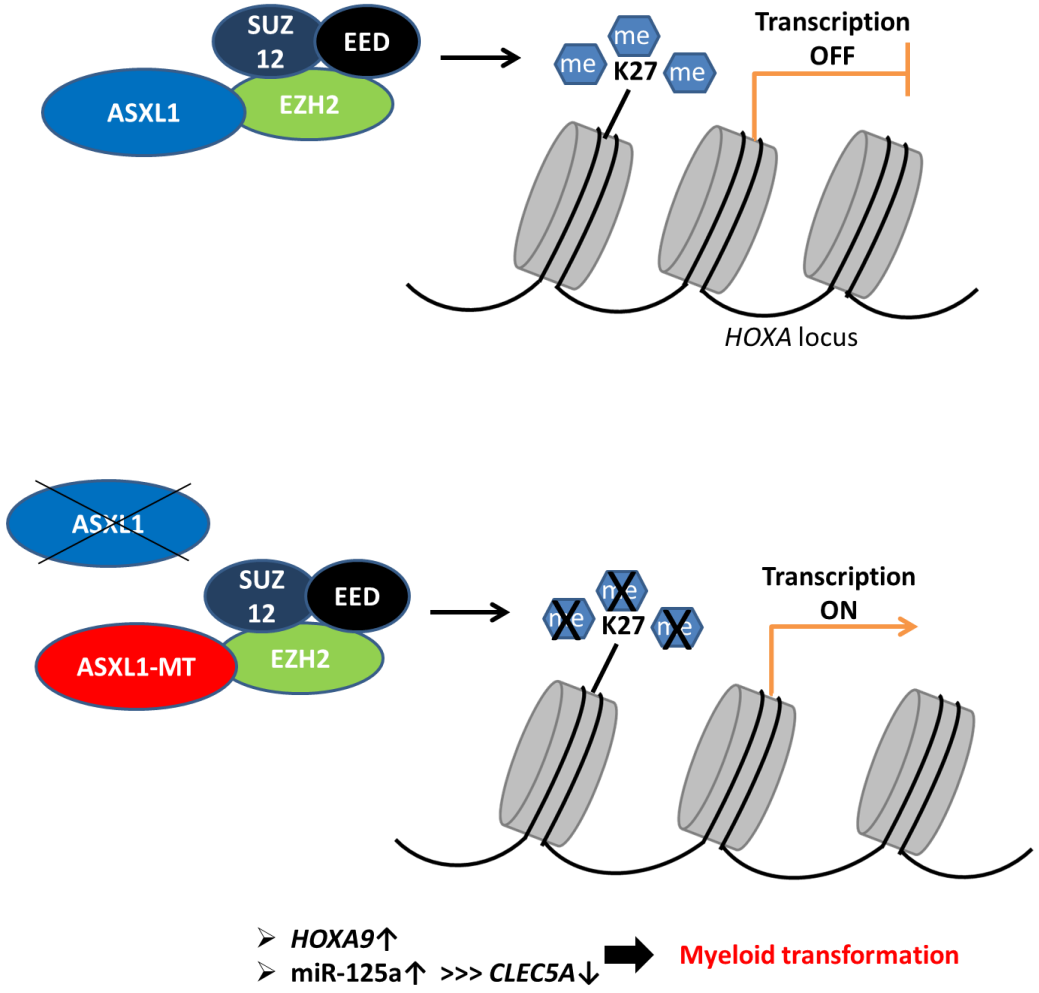

Figure 58. Schematic chart of the results in our experiment. In normal bone marrow, ASXL1-WT proteins bind to EZH2 and support PRC2 function to repress transcription in *HOXA* locus (upper figure). On the other hand, in the bone marrow of MDS patients with heterozygous *ASXL1* mutation, ASXL1-MT proteins inhibit the binding of ASXL1-WT to EZH2, leading to impairing PRC2 function (lower figure). Consequently, the loss of H3K27me3 modification results in derepression of *HOXA9* and miR-125a. Also, miR-125a prevents the transcription of *CLEC5A*, which is required for myeloid differentiation. These data suggest ASXL1-MT plays a critical role in myeloid transformation.

Table 1. Sequence of shRNA for *Clec5a*

sh1 top	GATCCGGAACAGTCTGTCCCAGAAACTTCAAGAGAGTTTCTGGGACAGACTGTTCCTTTTTTGGAAAG
sh1 bottom	AATTCTTTCCAAAAAAGGAACAGTCTGTCCCAGAAACTCTCTTGAAGTTTCTGGGACAGACTGTTCCG
sh2 top	GATCCGGATTATTGTGCAACACAAGGTTCAAGAGACCTTGTGTTGCACAATAATCCTTTTTTGGAAAG
sh2 bottom	AATTCTTTCCAAAAAAGGATTATTGTGCAACACAAGGTCTCTTGAACCTTGTGTTGCACAATAATCCG
sh3 top	GATCCGGATCAACAACTCTGTGTTCATTCAAGAGATGAACACAGAGTTGTTGATCCTTTTTTGGAAAG
sh3 bottom	AATTCTTTCCAAAAAAGGATCAACAACTCTGTGTTCATCTCTTGAATGAACACAGAGTTGTTGATCCG
sh4 top	GATCCGGACATAGCTGGTATTGAGAATTCAAGAGATTCTCAATACCAGCTATGTCCTTTTTTGGAAAG
sh4 bottom	AATTCTTTCCAAAAAAGGACATAGCTGGTATTGAGAATCTCTTGAATTCTCAATACCAGCTATGTCCG

Table 2. qRT-PCR primers for mRNA expression

	Gene	Forward Primer Sequence	Reverse Primer Sequence
Human	***HOXA9***	CCACGCTTGACACTCACACT	CAGTTCCAGGGTCTGGTGTT
	CLEC5A	TCTTGGAATGAAAGCAGGGACTT	TTCAGTTTCTCTGGCGTGTTGACA
	ASXL1	GCCTCGAGTTGTCCTGACTC	TCTGTTGCGCTTCATTTGAC
	GAPDH	GAGCTGAACGGGAAGCTCACTGG	CAACTGTGAGGAGGGGAGATTCAG
Mouse	***Clec5a***	CCTTGGAAAGACAGCATGGATTA	ACTTCAGTTTCTCTGGAGTGTTGACA
	Hoxa5	CTCATTTTGCGGTCGCTATCC	ATCCATGCCATTGTAGCCGTA
	Hoxa9	GTAAGGGCATCGCTTCTTCC	ACAATGCCGAGAATGAGAGC
	Hoxa10	CCTGCCGCGAACTCCTTTT	GGCGCTTCATTACGCTTGC
	Gapdh	GCATTGTGGAAGGGCTCATG	TTGCTGTTGAAGTCGCAGGAG

Table 3. qPCR primers for ChIP-qPCR studies

Gene	Forward Primer Sequence	Reverse Primer Sequence
Hoxa5	TCGAGTCCGACTGAACGGCG	GTTGTCCAGTCGTAAATCCTGC
Hoxa10	AAACTCTGGCTCGGGATTGG	GAGCATGACATTGTTGTGGGAT
Hoxa9	GGAGGGAGGGGAGTAACAAA	AGTTTCTGGGCCCTGTATGA
Clec5a	CAGAAGTAGAAGTTCCCTTCCTCT	CTGCTCGGTAATGTCCTTGTT
miR-125a-1	GCACACAAGCTCGTGTCTGT	TCCTCAACTATACAACCTCCTAC
miR-125a-2	GTGCTGTGAATGTATCTCTGTG	GGTGGACCAGAAAAACCCTT
miR-125a-3	GACCCTTTAACCTGTGAGGA	GAGTTTCAAATGATGGTCAAGC